Technical Report on $\bar{p}p \to \omega\omega\pi^0$ at rest

1 Data Selection

1.1 Pre-selection

The data used in this analysis were selected from a total sample of ∼9.4M 4-prong triggered events: 2.1M from data-taking in June 1991, 1.0M from August 1991 and 6.28M from April 1996. Table 1 summarises the preselection of the data; the four-prong trigger requires four hits in at least one of the two mulitwire chambers (or Si vertex detector) and also hits in at least one of the first three layers of the drift chamber and at least one hit in one of the last four layers.

Using Crystal Barrel offline analysis code ∼2.4M events with four well reconstructed tracks and balanced charges (or golden tracks) were selected. The global tracking software was used to match energy deposits in the crystals due to charged particles with their corresponding tracks in the drift chamber and multiwire chambers.

Next, photons were defined as any unmatched (i.e. no corresponding track due to a charged particle) energy deposit in the crystals with an energy of at least 10 MeV. Any event with an energy shower which had a central crystal of type-13 were rejected - thus rejecting events where energy could have been lost down the beam pipe. Events with < 25 photons were selected leaving a data set of ∼1.3M events after preselection.

Selection	Events (M)
4-prongs triggered	9.38
4 golden tracks ($\Sigma q = 0$)	2.54
Number of γ 0-24	1.28

Table 1: Pre-selection

A Monte Carlo sample of 1.034M events of the type $p\overline{p} \to \omega\omega\pi^o$ (where both ω decay to $\pi^+\pi^-\pi^o$) was generated using CBgeant.

1.2 Kinematic fits

The surviving events were submitted to a 7C kinematic fit to $2\pi^+2\pi^-3\pi^o$; 11,679 events survived a 0.1% confidence level cut. 11,610 Monte Carlo events passed this cut. Figures 3 and 4 show the resulting confidence level distributions for data and Monte Carlo.

The $\pi^+\pi^-\pi^o$ invariant mass distribution after the fit to $2\pi^+2\pi^-3\pi^o$ is shown in figure 5. Clear signals due to the ω and η mesons can be seen.

Next a 9C kinematic fit to $\omega\omega\pi^o$ (ω decaying to $\pi^+\pi^-\pi^o$) was performed on these data and a cut made at the 5% confidence level. This left 1882 data and 6894 Monte Carlo events. The confidence level distributions after this cut at the 5% level are shown in figures 6 and 7. Figure 8 shows the $\pi^+\pi^-\pi^o$ invariant mass distribution; after the fit to $\omega\omega\pi^o$ the η signal has disappeared.

1.3 Combinatorics

The kinematic fit to $\omega\omega\pi^o$ has 180 different possible combinations of particles giving $\omega\omega\pi^o$. It is possible that in some cases the confidence level of an incorrect combination will be higher than that of the correct combination. Monte Carlo data were used to estimate the level of combinatorics in the sample. The Monte Carlo study gave a 25% level of wrong combinations chosen by the fit. Here there are some discrepencies between data and Monte Carlo - in general a Monte Carlo event was found to be more likely than a real event to have more than one combination with a confidence level above the cut. Hence it is likely that the level of combinatorics is lower in the data.

Ways of reducing the combinatorics were studied using Monte Carlo events. For those events which had two or more combinations, if the ratio of confidence level for the best combination to that of the second best combination was greater than 0.6, then it was more likely that the wrong combination had been chosen. It was also found that events with more combinations above the confidence level cut had more wrong combinations. Using this information two cuts were introduced. The first was that the total number of combinations of the event be < 3. The second was that the ratio of the confidence level of the best combination to that of the second best combination be < 0.6.

It is found that the combinatorical background in the sample after these cuts is <16%.

1.4 Background

A possible source of background to $\omega\omega\pi^o$ is the $\omega\pi^+\pi^-2\pi^o$ channel, where the π^+, π^- and one of the π^o are misidentified as coming from the decay of an ω. To investigate this, all possible combinations of $\pi^+\pi^-\pi^o$ were formed and the best omega (the one with invariant mass closest to the mass of the ω given by the Particle Data Group [10]) was selected. Then the invariant mass distribution of the second best combination was plotted. Figure 9 shows this distribution. A dip can be seen at the ω mass. This is because any combinations at this mass will be selected as the best one. Comparing with the distribution from the Monte Carlo (figure 10), it can be seen that the distributions are in general very similar, but in the data there are some events outside the ω peak. The events in these tails make up 4% of the sample. They are most probably background from $\omega\pi^+\pi^-2\pi^o$. Hence a cut was introduced to eliminate these events: that the invariant mass of the second best omega combination be $> 752\ \ MeV$ and $< 812\ \ MeV$.

1.5 Charged pion identification

One last cut was introduced due to an error in the CB software. The order of particles in the kinematic fit bank is not always that of the hypothesis card: occasionally the π^+ and π^- from an ω are interchanged. A cut was introduced to ensure the identities of these particles. This gives a final data set of 1346 events and 4677 Monte Carlo events. Table 2 gives a summary of the data selection.

Cut	Data	M. Carlo
Kinematic fit to $2\pi^+2\pi^-3\pi^o$ 0.1%	11679	11610
Kinematic fit to $\omega\omega\pi^o$ 5%	1882	6894
No. of combinations $<$ 3	1740	5733
Ratio of 2nd best/best $<$ 0.6	1563	5160
$752\ MeV <$ S(second best ω) $<$ $812\ MeV$	1503	5109
Charge of π^+/π^-well defined	1346	4677

Table 2: Summary of Data Selection

2 Branching ratio $p\overline{p} \rightarrow \omega\omega\pi^o$

Because of worries about the accuracy of the Monte Carlo in determining the reconstruction efficiency, the branching ratio of $p\overline{p} \rightarrow \omega\eta\pi^o$ was used to normalise our data and find the branching ratio of $p\overline{p} \rightarrow \omega\omega\pi^o$.

A Crystal Barrel analysis of 7γ [1] found the branching ratio of $p\overline{p} \rightarrow \omega\eta\pi^o$ to be $(0.68 \pm 0.01 \pm 0.05)\%$. Figure 5 illustrates the mass spectrum of $\pi^+\pi^-\pi^0$ combinations. We estimate 930 ± 50 $\eta\omega\pi^0$ events and 2000 ± 50 $\omega\omega\pi^0$.

Correcting for the branching ratios: BR$[\omega \rightarrow \pi^+\pi^-\pi^o]$=$0.888 \pm 0.007$ and BR$[\eta \rightarrow \pi^+\pi^-\pi^o]$=$0.274 \pm 0.026$, the branching ratio for $p\overline{p} \rightarrow \omega\omega\pi^o$ (for all possible decay modes) was found to be $(0.45 \pm 0.07) \times 10^{-3}$.

3 Monte Carlo acceptance

Figure 11 shows the Dalitz plot of the Monte Carlo data, the acceptance appears to be flat across the whole of phase space, except for an obvious loss in edge bins. There, the fitting procedure allows for the available bin size within the boundary of the Dalitz plot.

4 Discussion of AX

The first confirmed sighting of $f_2(1565)$ was made by the ASTERIX collaboration in data on $p\overline{p} \rightarrow \pi^+\pi^-\pi^o$[2, 3]. A clear signal was observed in the $\pi^+\pi^-$ invariant mass without any corresponding signal in $\pi^+\pi^o$ or $\pi^-\pi^o$; this suggested an isoscalar resonance. By fitting with the standard Breit Wigner form of the amplitude, they found a resonance mass of 1565 MeV and a width of 170 MeV. An analysis of the decay angular distribution strongly suggested spin 2. This resonance, which they called the AX, was only observed in annihilation from initial $\bar{p}p$ P-states.

Subsequently the same resonance was observed with almost identical mass and width in Crystal Barrel data on $p\overline{p} \rightarrow 3\pi^o$ by Anisovich et al. [4]. Their analysis was confirmed by a subsequent similar analysis of Crystal Barrel data with higher statistics [5]. Meantime, it was observed by the Obelix experiment in $\overline{n}p \rightarrow \pi^-\pi^+\pi^+$[6].

The next step was a combined analysis of Crystal Barrel data on $3\pi^o$, $\eta\eta\pi^o$ and $\eta\pi^o\pi^o$ by Abele et al. [7]; it revealed a definite cusp in the $J = 2$ $\pi\pi$ amplitude at the $\omega\omega$ threshold. The strong coupling to $\omega\omega$ allowed the

AX to be identified with a resonance observed earlier by GAMS [8] and VES [9] in decays to $\omega\omega$, just above the $\omega\omega$ threshold; they denoted that resonance as $f_2(1640)$ and it is still listed as such by the Particle Data Group [10].

The present analysis will show that all these observations may be fitted consistently with a single resonance, using a Flatté form for the amplitude including the s-dependence of the coupling to $\rho\rho$ and $\omega\omega$. It includes the VES $\omega\omega$ data [9] as a constraint on the width. These data have a better mass resolution than GAMS data, so are chosen in preference. The parameterisation for the AX derived in this thesis may now be used in future analyses.

5 Amplitude Analysis

The amplitude analysis of the data described in earlier chapters will now be described. Figures 12, 13 show the mass projections for $\omega\pi^o$ and $\omega\omega$. The points with error bars are the data and the histogram shows phase space. In the $\omega\omega$ projection, there is an obvious enhancement around 1600 MeV.

Figure 14 shows the Dalitz plot for the data. There is a clear peaking of events towards the top right hand edge. This suggests the presence of either (or a combination of) $f_2(1565)\rightarrow\ \omega\omega$, $f_0(1500)\rightarrow\ \omega\omega$, or $b_1(1235)\omega$. One can attempt to distinguish between these three possibilities using angular correlations for production and decay of the two ω.

Therefore in the amplitude analysis the primary processes considered were:

$$
\begin{array}{ll}
^1S_0 & \rightarrow f_0(1500)\pi^o \\
 & \rightarrow f_0(1750)\pi^o \\
 & \rightarrow \sigma\pi^o \\
 & \rightarrow b_1(1235)\ \omega \\
 & \rightarrow [f_2(1565)\pi^o]_{\ell=2} \\
^3P_2 & \rightarrow [f_2(1565)\pi^o]_{\ell=1} \\
^3P_1 & \rightarrow [f_2(1565)\pi^o]_{\ell=1}
\end{array}
$$

The orbital angular momentum of the final state in the production process is denoted by ℓ. The state denoted by σ is a slowly varying amplitude with quantum numbers 0^+ decaying to $\omega\omega$; it is parameterised as a constant amplitude. Later, 0^{-+}, 1^{-+} and 2^{-+} quantum numbers will also be discussed (section 5.6.2); they are less likely, since they require decays with $L = 1$, and there is little available phase space so close to threshold.

5.1 The fitting function

Because of the low statistics, a log likelihood fit was used. Let w be the fitted cross section for the kinematics of a particular event. Then the log likelihood function (S) is defined as

$$S = -ln\ L = N(ln \sum_{i=1}^{M} w_i) - (\sum_{j=1}^{N} ln\ w_j) \tag{1}$$

where N is the number of data events and M the number of Monte Carlo events. A minimum value of S indicates the best fit. With this definition of the likelihood function, a change of 0.5 in S corresponds to one standard deviation.

5.2 Form of the amplitudes

In the first instance, all resonances were treated as Breit-Wigner amplitudes with constant widths. The Breit-Wigner parameterisation used is given in equation 2:

$$BW(s, m, \Gamma) = \frac{m\Gamma}{s - m^2 + im\Gamma}. \tag{2}$$

Here $BW(s, m, \Gamma)$ is the amplitude, m is the mass and Γ is the width. For all resonances other than the AX, we use values given by the Particle Data Group [10].

Annihilation at rest may procede from the initial $^1S_0$ state with $\ell = 2$ in the production process, or from $^3P_1$ and $^3P_2$ with $\ell = 1$. These processes are inhibited by centrifugal barriers. For these, the standard Blatt-Weisskopf (Hippel-Quigg) forms are used. For $\ell = 2$, the barrier takes the form

$$CB(\mathbf{P}, R, 2) = \frac{\mathbf{P}^2}{\mathbf{P}^2(\mathbf{P}^2 + F) + F^2} \tag{3}$$

and for $\ell = 1$

$$CB(\mathbf{P}, R, 1) = \sqrt{\frac{\mathbf{P}^2}{\mathbf{P}^2 + F/3}}\ , \tag{4}$$

where $\mathbf{P}$ is the momentum of the resonance in the overall centre of mass; F is related to the radius R (in fm) by

$$F = \frac{0.1164}{R^2}. \tag{5}$$

Initially the radius of interaction was taken as 1 fm. A Vandermeulen form factor [16] for the production process was also included:

$$Y(s) = exp(-0.6(\sqrt{M_\omega^2 - (M_{\pi^0} + \sqrt{s})})). \tag{6}$$

This form factor accounts for the well known observation that final states with large momentum are suppressed; it is displayed in figure 15. The total amplitude for a particular process can be written as:

$$A = g \times CB(\mathbf{P}, R, \ell) \times Y(s) \times BW(s, m, \Gamma) \times T(\underline{n}_{\omega_1}, \underline{n}_{\omega_2}), \tag{7}$$

where g is a complex coupling constant to be determined by the fit. $T(\underline{n}_{\omega_1}, \underline{n}_{\omega_2})$ is a tensor containing the angular information for the particular process. It gives the vital information identifiying the spins and parities of contributing channels. It will be described in the next section.

5.3 $\underline{n_1}.\underline{n_2}$

The matrix element of the ω decay to $\pi^+\pi^-\pi^o$ depends explicitly upon the vector normal to the plane of this decay. Let $\vec{p_1}$ and $\vec{p_2}$ be the momentum vectors of π^+ and π^- in the rest frame of the ω. Then the matrix element for the decay is given [11] by the vector product

$$T = \vec{p_1} \wedge \vec{p_2}. \tag{8}$$

The spin information is thus given by the normal to the decay plane of the ω:

$$\vec{n} = \frac{\vec{p_1} \wedge \vec{p_2}}{|\vec{p_1} \wedge \vec{p_2}|}. \tag{9}$$

Figure 16 shows how this distribution would look for a 0^+ resonance and figure 17 shows how it would look for a 2^+ resonance. For 0^+ it has a $cos^2\phi$ form, where ϕ is the angle between $\vec{n_1}$ and $\vec{n_2}$. For 2^+, the distribution appears flatter. Figure 18 shows the $\underline{n_1}.\underline{n_2}$ distribution for the data. The distribution is flat at low $\underline{n_1}.\underline{n_2}$ as for 2^+ but then begins to rise, as for 0^+. It appears to be a combination of both. Hence there are both 2^+ and 0^+ contributions in the data.

The expressions for T describing resonance production from $^3P_2$ and $^3P_1$ initial states have a complicated form involving correlations of the decay planes of both ω's and their momenta (see appendix 1 for a discussion

of these expressions). The fit is sensitive to these expressions but it is not possible to display this dependence graphically in any simple way. However the fit is able to determine the contributions from $^3P_2$ and $^3P_1$ accurately. This will become evident in the tables which follow.

5.4 Initial fit

In fitting the data, it had to be taken into account that the process $^1S_0 \rightarrow (0^+)\pi^0$ involves no orbital angular momentum and therefore has no dependence on the angle θ between the decay ω and the direction of the resonance. Likewise, the process $p\overline{p} \rightarrow b_1(1235)\omega$ involves no angular dependence on θ for S wave decays of $b_1(1235)$; the D wave decay amplitude is also included using the Particle Data Group [10] value for the D/S ratio, but is small. Because of this lack of angular dependence, $f_0(1500)\pi^o$ and $b_1(1235)\omega$ give similar angular distributions. If both are included in the fit, they both become very large, but with a cancelling destructive interference between them. This is a well known numerical instability. Table 3 shows the contributions and interference terms from a fit including both $f_0(1500)$ and $b_1(1235)$; the diagonal terms are the percentage intensities and the other terms are the real and imaginary parts of the interference; the real part is in the lower left corner and the imaginary part in the upper right corner.

$f_0(1500)$	**218.66**	-15.58
$b_1(1235)$	-212.09	**109.02**

Table 3: Contributions (%) and interference between $f_0(1500)$ and $b_1(1235)$

Likewise, because of the restricted mass range for $\omega\omega$, $f_0(1750)$ is very similar to σ. Again they give large contributions to the fit with a cancelling destructive interference between them. Table 4 shows the contributions and interference terms from a fit including both $f_0(1750)$ and σ.

$f_0(1750)$	**129.69**	-101.05
σ	-324.64	**396.01**

Table 4: Contributions (%) and interference between $f_0(1750)$ and σ

These large destructive interferences appear unphysical, and some simplification to the fit is required. Table 5 gives a summary of some of the fits which have been tried. It can be seen immediately that the data definitely demand P-state annihilation and hence a 2^+ contribution. No tolerable fit could be achieved without the inclusion of $f_2(1565)$. The 0^+ contribution proved more difficult to determine, because of the large and unphysical interferences between the different components. The Dalitz plot for the data has horizontal and vertical bands which suggest $b_1(1235)$, and in fact the best fit was achieved by including $b_1(1235)$ and the σ together. In conclusion, we can fit with either $f_0(1500)$ or $b_1(1235)$ but not both together; the $b_1(1235)$ is preferred.

$f_0(1500)$	$f_0(1750)$	σ	$b_1(1235)$	$^1S_0 \rightarrow f_2(1565)$	$^3P_2 \rightarrow f_2(1565)$	$^3P_1 \rightarrow f_2(1565)$	S
11.60	79.10	-	-	-	-	-	+586.8
61.53	18.57	-	-	16.92	-	-	+140.2
23.51	16.62	-	-	2.69	24.39	16.91	-54.3
60.22	-	-	-	1.94	22.20	15.25	-27.3
11.39	-	21.13	-	2.76	24.75	17.25	-55.9
-	-	48.29	-	3.14	28.31	19.98	-50.5
-	-	120.13	136.83	-	-	-	+285.4
-	-	67.10	69.64	13.85	-	-	+230.8
-	-	76.01	63.49	3.51	27.81	16.92	-84.8
-	14.01	-	26.75	2.84	32.68	20.07	-38.1
-	63.61	-	-	4.15	15.90	16.02	-24.6

Table 5: Contributions (%) and S of some initial fits

5.4.1 $f_0(1500)$

The evidence for $f_0(1500)$ in the data is weak; when introduced as the only 0^+ resonance, it does not give a good fit nor does it give a better fit than the $b_1(1235)$ and σ when it is in combination with $f_0(1750)$ or σ.

A large contribution from $f_0(1500)$ seems unlikely, since there is evidence from other data that the branching ratio of $f_0(1500) \rightarrow \omega\omega$ is small. Firstly, data on $J/\Psi \rightarrow \gamma(4\pi)$ [12] require that $f_0(1500)$ decays dominantly to $\sigma\sigma$ rather than $\rho\rho$; at the quark level, coupling to $\rho\rho$ is required to be three times that to $\omega\omega$, implying that $f_0(1500) \rightarrow \omega\omega$ will be small. Also, in the Crystal Barrel analyses of $p\overline{p} \rightarrow 3\pi^o$ [3,4,6], there is no indication of any cusp in the amplitude of $f_0(1500)$ at the $\omega\omega$ threshold. Thirdly, analysis of Crystal Barrel data on 5π final states at rest [13] provides evidence for $f_0(1500) \rightarrow \sigma\sigma$, but none for decays to $\rho\rho$. ¿From this information, it is estimated that the branching ratio of $f_0(1500) \rightarrow \omega\omega$ is $< 4\%$ of that to $\pi\pi$.

The branching ratio of $p\overline{p} \rightarrow f_0(1500)\pi^o$ with $f_0(1500)$ decaying to $\pi\pi$ was found to be $\simeq 2.45 \times 10^{-3}$ from the analysis of Crystal Barrel data on $3\pi^o$. Hence the $f_0(1500) \rightarrow \omega\omega$ amplitude must be small in the $\omega\omega\pi^o$ data and it is therefore dropped from the analysis.

5.4.2 $f_0(1750)$

In the case of $f_0(1750)$ when combined with $b_1(1235)$, a worse fit is obtained then fitting with it alone and, as stated before, when introduced with the σ huge destructive interference occurs. Therefore $f_0(1750)$ is omitted.

5.4.3 σ and $b_1(1235)$

Neither the σ or $b_1(1235)$ can account for the 0^+ contribution by themselves nor in combination with the $f_0(1500)$ or the $f_0(1750)$. When introduced together, a much more reasonable fit is obtained. The interferences are relatively large but do not seem unphysical. S is much improved.

5.4.4 $f_2(1565)$

As stated before, $f_2(1565)$ is necessary in the fit. Annihilation from the P-state to $f_2(1565)$ improves S by a large amount ($\Delta S = 370$). Annihilation from $^1S_0$ also improves the fit significantly (although its contribution is small), $\Delta S = 55$. It is interesting to note that for all fits the contributions from $^3P_2$ and $^3P_1$ remain stable at around 25% for $^3P_2$ and 15% for $^3P_1$, no matter what additional 0^+ contribution is included; this is because the angular information determines accurately the contribution from $^3P_2$ and $^3P_1$. The $^1S_0$ contribution also remains relatively stable at around 3–4%. Figure 19 shows the fit achieved when including $f_2(1565)$, $b_1(1235)$ and σ. The fit is tolerable but it peaks too low in $\omega\omega$ mass. We shall refer to this fit from now on as the reference fit. Table 6 shows the contributions from 0^+ in the fit and their interferences (the diagonal elements are the contributions in percent and the off diagonal terms are the real and imaginary parts of the interferences).

5.5 Slices

As a check on the components in the fit, the data have been divided into four slices of $\omega\omega$ invariant mass. The mass range of each slice is chosen to contain

$^1S_0$	**3.51**	-0.18	0.01
$b_1(1235)$	-0.53	**63.49**	-46.76
σ	0.81	-41.08	**76.01**

Table 6: The contributions (%) from $b_1(1235)$ and σ and interference terms

approximately the same number of events. Each slice was then fitted with four components: $\sigma\pi$, $^1S_0 \to AX$, $^3P_1 \to AX$ and $^3P_2 \to AX$. The objective was to look more closely at the contribution from the $f_2(1565)$. The $b_1(1235)$ contribution was not included, as there is not sufficient range of s to isolate it from σ. Table 7 gives the range of these slices and the number of events contained in each one.

Lower bound (GeV^2/c^4)	Upper bound (GeV^2/c^4)	No. of events
0.0	2.568	334
2.568	2.665	338
2.665	2.790	338
2.790	4.000	336

Table 7: Number of events in each slice of $s(\omega\omega)$

Table 8 gives the contributions from $f_2(1565)$ and σ in each of the slices. In the first mass slice, the $^1S_0$ contribution of $f_2(1565)$ is high but in the fourth slice this contribution drops significantly. This is expected, since the angular momentum barrier should inhibit $^1S_0$ production in this mass region. The $^3P_2$ and $^3P_1$ contributions are lower in the first slice but then consistent across the other slices. The projections for these slices can be seen in figures 20, 21, 22 and 23.

5.6 Improving the fit

5.6.1 Mass and width of $f_2(1565)$

The projections for the reference fit (figure 19) show that the fit peaks at too low a mass in the $\omega\omega$ projection. This projection can be greatly improved with a corresponding improvement in S if either the mass or the width of

s^2 (GeV^2/c^4)	σ	$^1S_0 \rightarrow f_2(1565)$	$^3P_2 \rightarrow f_2(1565)$	$^3P_1 \rightarrow f_2(1565)$	S
0.000 - 2.568	52.87	11.33	23.62	10.46	-620.0
2.568 - 2.665	48.84	3.55	29.30	19.32	-559.0
2.665 - 2.790	44.84	6.21	27.01	21.75	-504.5
2.790 - 4.000	44.49	3.39	31.71	20.76	-311.3

Table 8: Contributions (%) to the fit for the different slices of s

$f_2(1565)$ is increased. Tables 9 and 10 detail the effect of varying the width and mass of $f_2(1565)$.

It can be seen that the best improvement is acheived by increasing the width. S increases significantly (ΔS=33.6) if the width is increased to 202 MeV; any further increase is insignificant. Figure 24 shows the corresponding projections; the $\omega\omega$ projection is greatly improved.

Γ MeV	σ	$b_1(1235)$	$^1S_0 \rightarrow f_2(1565)$	$^3P_2 \rightarrow f_2(1565)$	$^3P_1 \rightarrow f_2(1565)$	S
102	76.28	63.88	3.46	27.80	16.96	-84.8
127	72.17	62.04	3.76	29.36	18.25	-100.0
152	68.48	60.69	4.06	30.38	19.21	-109.3
177	65.24	59.68	4.32	31.09	19.92	-115.0
202	62.41	58.87	4.57	31.59	20.45	-118.4
227	60.02	57.94	4.77	31.98	20.82	-120.4
252	58.00	57.58	4.94	32.24	21.13	-121.5

Table 9: Varying the width of $f_2(1565)$

Increasing the mass also improves S, but the fit is not really as good as that achieved by increasing the width. The projections for a mass of 1605 MeV are shown in figure 25. The Dalitz plot looks better, but the $\omega\omega$ projection, although improved from the reference fit, is not too well fitted.

5.6.2 Other possibilities

The results found from this initial analysis of $p\overline{p} \rightarrow \omega\omega\pi^o$ seem reasonable. A definite 2^+ contribution is required by the data; a resonance around 1565 MeV with a width of 202 MeV is preferred. This resonance contributes about 50% of the total. The 0^+ sector is less well determined, but this does not have

Mass MeV	σ	$b_1(1235)$	$^1S_0 \rightarrow f_2(1565)$	$^3P_2 \rightarrow f_2(1565)$	$^3P_1 \rightarrow f_2(1565)$	S
1575	76.55	64.89	3.51	28.36	17.10	-90.0
1585	75.95	65.65	3.70	29.05	17.40	-97.0
1595	74.40	66.37	4.02	29.64	17.85	-103.7
1605	72.09	67.59	4.50	29.94	18.42	-108.3
1615	69.05	69.52	5.16	29.89	18.99	-109.4

Table 10: Varying the mass of $f_2(1565)$

an effect on contributions from the AX. But before moving on to investigate the properties of the AX in more detail, it is necessary to check for the presence of more unlikely resonances first. It is possible for 0^{-+},1^{-+} and 2^{-+} resonances to decay to $\omega\omega$ with $L = 1$ in the decay. The 1^{-+} is exotic and hence evidence for its presence would have to be very strong; it is inhibited by centrifugal barriers for production and decay to $\omega\omega$. The 0^{-+} and 2^{-+} are also inhibited by an $L = 1$ centrifugal barrier for decay.

Firstly it was found that none of these resonances can fit the data without the presence of $f_2(1565)$, so the next thing to check was whether or not any of these resonances could significantly improve the fit already obtained. Table 11 shows the contributions from each channel and changes in likelihood for the inclusion of these resonances (with masses of 1650 MeV and widths of 250 MeV), added to the reference fit.

$^1S_0 \rightarrow f_2(1565)$	$^3P_2 \rightarrow f_2(1565)$	$^3P_1 \rightarrow f_2(1565)$	0^{-+}	2^{-+}	$^1S_0 \rightarrow 1^{-+}$	$^3P_1 \rightarrow 1^{-+}$	ΔS
4.59	31.19	17.39	-	-	0.07	3.09	4.7
4.75	27.13	16.79	-	7.68	-	-	8.9
4.77	29.33	19.45	3.21	-	-	-	4.2

Table 11: Percentage contributions for fits including 0^{-+}, 1^{-+} and 2^{-+}

The evidence for the presence of 1^{-+} and 0^{-+} is not convincing; a change in S of 4 is not significant. For 2^{-+} the change in S is 9, which is a little more significant. A scan of the mass reveals that it peaks at around 1900 MeV with a width of 230 MeV. This small change in S is not sufficient to suggest the presence of a new resonance, hence it seems likely that the fit is using the 2^{-+} amplitude to resolve minor problems at high $\omega\omega$ mass. Hence these possibilities can be discounted.

5.7 Investigation of $f_2(1565)$

Up to now we have used a Breit Wigner amplitude with constant width for the AX. But we know from CERN-Münich data [15] that $\Gamma_{\pi\pi}$ is in fact small, much smaller than $\Gamma_{\omega\omega}$ and Γ_{tot}. Hence it is appropriate to use a Flatté form for the amplitude which includes the s dependence of the partial widths and of the mass.

The amplitude we use is:

$$f_{1565} = \frac{gB_L(p)Y(p)\exp(-\alpha q^2)}{M^2 - s - m(s) - iM\Gamma_{tot}}, \quad (10)$$

$$\Gamma_{tot} = \Gamma_{2\pi} + g_1\rho_1 + g_2\rho_2. \quad (11)$$

In the numerator of equn. (10), $Y(p)$ is the Vandermeulen form factor [16] for the production process $\bar{p}p \to f_2(1565)\pi$, in terms of the centre of mass momentum p with which the resonance is produced. The factor $B_\ell(p)$ is the standard Blatt-Weisskopf centrifugal barrier factor for production with orbital angular momentum ℓ; for the ${}^1S_0$ initial state, $\ell = 2$ and for ${}^3P$ initial states, $\ell = 1$. The factor g is a complex coupling constant for ${}^1S_0$ production, and for P-state production may be taken to be real, since only $f_2(1565)$ contributes. The exponential is a form factor for decay of the resonance to ω of momentum q, with $\alpha = 1.5$ GeV^{-2}. This value of α is taken from general experience in fitting other data and corresponds to a radius of interaction of 0.6 fm.

In equn. (11), the 2π width is taken to be constant. It is necessary to take care over the s-dependence of the widths for decays to $\rho\rho$ and $\omega\omega$. The factors $\rho_{1,2}$ of equn. (11) are phase space factors for $\rho\rho$ (channel 1) and $\omega\omega$ (channel 2). For the $\omega\omega$ channel $\rho = 2q\exp(-2\alpha q^2)/\sqrt{s}$, where q is the momentum of the ω in the rest frame of the resonance and α is given above. For the $\rho\rho$ channel, the phase space factor is evaluated numerically using the model of Bugg, Sarantsev and Zou [14, equn.(40)]:

$$\rho_{\rho\rho}(s) = \int_{4m_\pi^2}^{(\sqrt{s}-2m_\pi)^2} \frac{ds_1}{\pi} \int_{4m_\pi^2}^{(\sqrt{s}-\sqrt{s_1})^2} \frac{ds_2}{\pi} \frac{8|\mathbf{p}|\,|\mathbf{p_1}|\,|\mathbf{p_2}|}{\sqrt{s\,s_1\,s_2}} |T_1(s_1)|^2 |T_2(s_2)|^2 \times exp(-\alpha|\mathbf{p}|^2) \quad (12)$$

where $\mathbf{p_1}$ and $\mathbf{p_2}$ are the momenta of the pions from the decay of each resonance in its rest frame and $\mathbf{p}$ stands for the momenta of the ρ in the centre

of mass frame. Factors of the form $|T_1(s)|^2$ are the squared amplitudes of the ρ mesons and are:

$$|T(s)|^2 = \frac{M\Gamma_1(s)}{(M^2 - s)^2 + (M\Gamma_1(s))^2}. \tag{13}$$

The phase space factors are illustrated in Fig. 26. The $\rho\rho$ phase space falls above $s = 3.6$ GeV^2 because of the form factor. Over the mass range of interest, up to 1.8 GeV, the form factor has only a small effect. The $\omega\omega$ phase space rises very rapidly from threshold, but also over the mass range of interest the form factor has little effect.

The value of g_1 in equn. (11) expresses the width for the $\rho\rho$ channel in the hypothetical limit $\rho \to 1$ and g_2 describes the $\omega\omega$ width in the same limit. The quark model predicts $g_1 = 3g_2$, corresponding to the three charge states of $\rho\rho$ and one for $\omega\omega$. The phase space illustrated in Fig. 26(a) has been parametrised, for convenience in fitting data, by the following expression:

$$\rho_{\rho\rho}(s) = \frac{(-3.909 + 10.571s - 1.81s^2)/48.47}{1 + exp(11.353 \times (1.063 - s) + s^2(4.572 - 0.826s)} \tag{14}$$

In equn. (11), $m(s)$ is a dispersive correction to the mass, evaluated from the subtracted dispersion relation:

$$m(s) = (s - M^2) \int \frac{ds'\ M\Gamma_{tot}(s')}{\pi(s' - s)(s' - M^2)}. \tag{15}$$

Here, Γ_{tot} is the total width appearing in the denominator of equn. (11). This dispersive correction makes the amplitude fully analytic. This has been checked by evaluating the standard dispersion relation for the real part of the amplitude in terms of an integral over its imaginary part; this relation is accurately satisfied over the whole range of s relevant here. The form of $m(s)$ is illustrated in figure 27.

5.8 Fits

Using this amplitude to fit the $\omega\omega\pi^o$ data gives a definite improvement, both in S and visually, when compared to the reference fit ($\Delta S = 37$). It solves in a natural way the problem of fitting the lower part of the $\omega\omega$ mass projection. But there are many unknown quantities - the values to be used for g_1, g_2, and $\Gamma_{\pi\pi}$.

It turns out that the fit to $\omega\omega\pi^0$ data is quite insensitive to the values of the mass, g_1, g_2 and $\Gamma_{\pi\pi}$. The $\omega\omega\pi^o$ data prefer a slightly higher mass around 1600 MeV for the $f_2(1565)$ with this form of the amplitude. Varying the width has very little effect; in fact, taking g_2 from 200 MeV to 800 MeV changes S by only 0.9. The fit prefers a value around 430 MeV. Because of this insensitivity to the width, we find it desirable to use the VES data [9] to provide an upper limit on the width. For $\Gamma_{\pi\pi}$, the CERN-Münich [15] limit of 30 MeV was used in initial fits. The contributions of $f_2(1565)$ from $^1S_0$,$^3P_2$ and $^3P_1$ remained relatively unchanged in all fits at around 4-5%, 30-31% and 19-20% respectively. Figure 28 shows the projections and Dalitz plots for a fit with $M = 1610\,MeV$, $g_2 = 430\,MeV$ and $\Gamma_{\pi\pi} = 30\,MeV$. To make better determinations of these unknown quantities it is necessary to use information about the AX from previous work. For this reason a combined fit has been made with Crystal Barrel data on $3\pi^o$. We first review those earlier fits.

5.9 Earlier fits to $3\pi^0$ data

In Crystal Barrel data on $p\overline{p} \rightarrow 3\pi^o$, V.V. Anisovich et al. [4] found evidence for a 2^+ resonance above the $f_2(1270)$ mass. It was needed in order to fit the edges of the Dalitz plot near $cos(\theta) = \pm 1$. They found a mass of 1.566 MeV and a width of 166 MeV.

In a later analysis by Abele et al. using higher statistics [7], it was found that χ^2 went up by 1000 if this $^3P_2$ resonance was omitted. The inclusion of the AX generated a second resonant loop in the Argand diagram of the $\pi\pi$ D-wave. At 1420 MeV, interferences with $f_2(1270)$ and $f_0(1500)$ were found to play a crucial role in fitting a conspicuous dip in the data. The resonance was found to have a definite cusp in its amplitude at the $\omega\omega$ threshold. For this reason, they included a partial width to $\omega\omega$. The inclusion of $\Gamma_{\omega\omega}$ improved χ^2 by 60, a significant amount. By including a form factor $exp(-\alpha p_\omega^2)$, the $\omega\omega$ mass spectrum observed by the $GAMS$ group could be reproduced, suggesting only one resonance decaying to both $\pi\pi$ and $\omega\omega$. This is the same resonance as is seen in the $\omega\omega\pi^o$ data of the present analysis.

However these two analyses only included annihilation to $f_2(1565)$ from the initial $\bar{p}p$ S-state. The inclusion of $f_2(1565)$ from $^3P_2$ and $^3P_1$ led to the fit becoming unstable. When the AX mass was left free, it drifted down to around 1480 MeV. The contribution from AX in P-state annihilation was found to be 8.4% from $^3P_2$ and 12.5% from $^3P_1$; considering how small

$\Gamma_{\pi\pi}$ is ($\leq$ 30 MeV from CERN-Münich data [15]), these contributions seem somewhat unlikely. It seemed that including P-state annihilation to AX was allowing minor defects to the background to be fixed; hence it was omitted from the published fit.

6 Outline of the combined fit

The $\omega\omega\pi^o$ data provide knowledge of the relative magnitudes of the contributions from $^1S_0$, $^3P_2$ and $^3P_1$ of $f_2(1565)$. These magnitudes are stable and independent of the other resonances included in the fit. It is now possible to use this information to limit the contribution from P-state annihilation to the AX in the $3\pi^o$ data and hence to find out more about this resonance.

The combined fit is made using the programme of Abele et al. to fit the $3\pi^0$ data. The components fitting this channel are

$$
\begin{aligned}
^1S_0 &\rightarrow \sigma\pi^0 && (16)\\
&\rightarrow f_0(1500)\pi^0 && (17)\\
&\rightarrow f_0(1300)\pi^0 && (18)\\
&\rightarrow f_0(980)\pi^0 && (19)\\
&\rightarrow f_2(1270)\pi^0 && (20)\\
&\rightarrow f_2(1565)\pi^0 && (21)\\
^3P_{1,2} &\rightarrow f_0(1270)\pi^0 && (22)\\
^3P_{1,2} &\rightarrow f_2(1565)\pi^0. && (23)
\end{aligned}
$$

It is not possible to fit $\omega\omega\pi^o$ and $3\pi^o$ data simultaneously using a Breit Wigner amplitude of constant width; the masses and widths are found to be inconsistent. This is due to the fact that the Breit Wigner amplitude does not model the s dependence of the amplitude correctly - in particular at the $\omega\omega$ threshold. However it is easy to obtain a consistent solution using the Flatté form described above. We can now use these two data sets to determine the mass of $f_2(1565)$, and can place some limit on $\Gamma_{\pi\pi}$.

In the first instance we set $g_1 = 3g_2$, as this is what is predicted for a $q\overline{q}$ state. It has been suggested [2, 3] that the AX is not a normal $q\overline{q}$ state and so we will investigate different relationships between g_1 and g_2. Also initially we set the radius of the centrifugal barrier to 1 fm.

There are two essential features which emerge from the combined fit. Firstly, the $3\pi^o$ data determine well the mass and full width of the AX;

the $\omega\omega\pi^o$ data depend only weakly on them. In earlier work, the dispersive correction $m(s)$ was not included. Introducing it greatly stabilises the determination of the mass. In earlier work, the imaginary part of the amplitude could be modified without corresponding changes to the real part. Now the amplitude is fully analytic, and real and imaginary parts of the amplitude are related rigorously. Suppose the mass changes in the fit. The value of $m(s)$ includes a subtraction at the resonance mass. The dispersion integral is evaluated at every iteration in the fit. Consequently, a change in the mass moves $m(s)$ bodily up or down at all values of s. The fit resists such changes, and the fit is stabilised.

Secondly, the contributions from $^1S_0$, $^3P_2$, $^3P_1$ to the $\omega\omega\pi^0$ data remain relatively unchanged for large changes in mass and/or width for the AX.

Tables 12 and 13 show the percentage contributions in this combined fit of the AX from $^1S_0$, $^3P_2$ and $^3P_1$ to $\omega\omega\pi^o$ and $3\pi^o$. The errors quoted are statistical and for $\omega\omega\pi^o$ correspond to a change of 0.5 in S or 1σ; for $3\pi^o$ they correspond to a change in χ^2 of 3, as a concession to the possibility of systematic errors in parametrising components in the fit. The contributions for $\omega\omega\pi^o$ are almost unchanged from the values obtained in all other fits. For $3\pi^o$ the total contribution of the AX (2.4%) is small. The contribution from P-state annihilation is restricted to small values, which have very little effect on the fit to $3\pi^0$. Those data are sensitive only to $^1S_0$ annihilation, since the AX interferes there with other strong components. The small contribution from $^1S_0$ helps to explain why the AX was not seen in S-state annihilation in the Asterix data on $\pi^+\pi^-\pi^o$[2]. An additional factor there is that $\rho\pi$ final states make a large contribution; these are absent in $3\pi^0$ data.

Initial state	contribution (%)
$^1S_0$	4.2 ± 0.2
$^3P_2$	19.5 ± 2.8
$^3P_1$	30.9 ± 3.3

Table 12: Percentage contributions of the AX for $\omega\omega\pi^o$ data

Figure 29 shows the resulting projections for $\omega\omega\pi^o$, S=-122.6. The value of the mass found for the AX is $1598 \pm 11\,MeV$ and the value for g_2 (and hence the width for the resonance in the $\omega\omega$ channel) is $435 \pm 30\,MeV$. Once again the errors quoted are statistical. Figure 30 shows the resulting Argand

Initial state	contribution (%)
$^1S_0$	0.50 ± 0.1
$^3P_2$	0.73 ± 0.07
$^3P_1$	1.22 ± 0.12

Table 13: Percentage contributions of the AX for $3\pi^o$ data

diagram for $3\pi^o$ data. $\Gamma_{\pi\pi}$ is found to be 2.4 MeV; this is a direct result of the small branching fraction of $f_2(1565) \to \pi^o\pi^o$, as we now show.

The total contribution of $f_2(1565)$ to $\pi^o\pi^o$ is $(0.50 \pm 0.1)\%$ from the initial $^1S_0$ state. Using this number and the known branching ratio for $p\overline{p} \to 3\pi^o$ of $(6.2 \pm 0.1) \times 10^{-3}$ [7], the branching ratio of $f_2(1565) \to \pi\pi$ may be found. Allowing for the 3 possible charge states ($\pi^+\pi^-$,$\pi^-\pi^+$,$\pi^o\pi^o$) a value of $(0.93 \pm 0.24) \times 10^{-4}$ is obtained.

7 Systematic uncertainties

The fit to $\omega\omega\pi^0$ data is over the $\omega\omega$ mass range 1564–1741 MeV. The fit to $3\pi^0$ data is sensitive to S-state annihilation and extends to $\pi\pi$ masses significantly below the $\omega\omega$ threshold. What uncertainties arise from the centrifugal barriers and form factors?

Figure 31 illustrates centrifugal barriers as a function of centre of mass momentum P for $\ell = 1$ (P-state annihilation) and $\ell = 2$ (S-state annihilation), using radii of interaction of 1 ± 0.4 fm. Although the $\omega\omega\pi^0$ data determine well the S and P-state contributions at high $\omega\omega$ masses, there is clearly significant uncertainty in extrapolating the relative S and P state contributions below the $\omega\omega$ threshold. Table 12 shows that $^3P_2$ annihilation is a factor 7 stronger than $^1S_0$, after integration over the $\omega\omega\pi^0$ data. However, for $3\pi^0$ data this factor falls to ~ 2.4. The difference arises from the strong s-dependence of the centrifugal barrier factor for $^1S_0$ annihilation. For an uncertainty of ± 0.4 fm in the radius of interaction, the P-state contribution of the AX to $3\pi^0$ data varies by a factor of 0.86-1.14. As regards the mass and width fitted to the AX, this has little effect, because the $3\pi^0$ fit is insensitive to a P-state component as small as this. There is, however, a strong effect on the fitted $\pi\pi$ width, which is discussed below.

Figure 32(a) shows the contribution in the $\omega\omega\pi^o$ data of $f_2(1565)$ from

$^1S_0$, (b) shows how the contribution would look if the centrifugal barriers were omitted, (c) and (d) show the contribution (with and without the barriers) from P-state annihilation. One sees clearly that the $\ell = 2$ centrifugal barrier suppresses (a) strongly at the higher masses. Comparing (c) and (d), the effect of the $\ell = 1$ barrier in P-state annihilation is evident.

Production of the AX it inhibited on its upper side, both in $3\pi^0$ data and $\omega\omega\pi^0$. This introduces uncertainty into the determination of the total width, which may increase without any large penalty in S. This is where VES data play a role, determining the upper side of the AX in an environment free of centrifugal barrier effects. These data restrict tightly the width to a small value. Imposing this constraint has little effect on the χ^2 of the fit to $3\pi^0$ data, affecting it by < 12.

7.1 The $\pi\pi$ width

The branching fraction for $^1S_0 \to f_2(1565)\pi$, $f_2 \to \pi^0\pi^0$ is quite well determined by the $3\pi^0$ data. The branching fraction of $^3P \to f_2(1565)\pi$, $f_2(1565) \to \omega\omega$ is well determined by $\omega\omega\pi^0$ data. However, the relative amounts of P and S-state annihilation depends strongly on the centrifugal barrier. This makes the determination of the relative $\pi\pi$ and $\omega\omega$ widths uncertain.

The branching fraction of $^1S_0 \to f_2(1565)\pi$, $f_2(1565) \to \omega\omega$ is determined with an error of $\sim 10\%$. However, extrapolating the $\ell = 2$ centrifugal barrier factor from the $\omega\omega$ mass range to that covered by $3\pi^0$ data is subject to an uncertainty of a factor of 3. Consequently, only a rough determination of the $\pi\pi$ width is possible, with this factor setting a scale. Changing the value of g_1/g_2 also has a small effect on the value of the mass and on $\Gamma_{2\pi}$; obviously the value of the ratio will alter the values found for g_1. The combined systematic error on the mass is found to be 9 $MeV$and on $\Gamma_{2\pi}$ it is a factor 3. Nonetheless, what emerges decisively is that the 2π width is very small.

7.2 The unfolded line-shape of the AX

There is one further consideration, which does not lead to any uncertainty. In $\bar{p}p$ annihilation, the cross section for production of the AX is inhibited by a phase space factor p/M, where p is the centre of mass momentum of the AX and M is its mass. It is necessary to unfold this factor in exhibiting the

line-shape of the AX, as it would appear in an environment not limited by the phase space for $\bar{p}p$ annihilation.

In order to study the sensitivity to these various factors, a small programme was constructed to plot out the line-shape of the AX as it appears (i) in isolation, (b) in P-state annihilation, (c) in S-state annihilation. Figure 33(a) shows the shape of the resonance in the 2π, $\omega\omega$ and $\rho\rho$ channels of $p\overline{p} \to$ annihilation from $^1S_0$. The 2π result is what is fitted to $3\pi^0$ data (scaled by a factor 5 for purposes of display). It peaks at 1.55 GeV with an asymmetric shape, falling to half-height at 1.59 GeV on the upper side, because of the rapidly opening $\omega\omega$ and $\rho\rho$ channels. The $\omega\omega$ result is likewise what is fitted to $\omega\omega\pi^0$ data. It peaks at 1.59 GeV, but is rapidly attenuated above that by the centrifugal barrier. The $\rho\rho$ channel peaks at the $\omega\omega$ threshold; it falls on the lower side because of the falling phase space and on the upper side because of the centrifugal barrier.

Figure 33(b) shows the corresponding estimate for an $f_2(1565)$ in isolation, without the effects of the limited phase space and the centrifugal barrier. The results are subject to considerable error of scale in unfolding the effect of the centrifugal barrier. Nevertheless it is interesting to note the cusp in the $\rho\rho$ channel which is clearly visible and is due to unitarity and the opening of the $\omega\omega$ channel. The $\rho\rho$ and $\omega\omega$ channels peak at ~ 1.66 and 1.63 GeV respectively.

By integrating branching fractions over the resonance, mean widths may be determined to each decay channel. Values are in the ratios

$$\overline{\Gamma}_{\pi\pi} : \overline{\Gamma}_{\omega\omega} : \overline{\Gamma}_{\rho\rho} = 0.06^{+0.12}_{-0.01} : 1.23 : 3. \tag{24}$$

There is a factor 3 uncertainty in $\overline{\Gamma}_{\pi\pi}/\overline{\Gamma}_{\rho\rho}$ due to uncertainties about the centrifugal barrier. The relative width to $\rho\rho$ and $\omega\omega$ is a matter of assumption, based on the expected ratio of coupling constants $g_1 = 3g_2$.

There are two interesting things to note from equn. [24]. The first is that it is clear that the width to 2π is very small, explaining why $f_2(1565)$ has not been seen in $\pi\pi \to \pi\pi$, e.g. in the CERN-Münich experiment [15]. The second is that the ratio of the widths of $\rho\rho$ to $\omega\omega$ is slightly above the value of 3 assumed from the quark model for g_1/g_2. An explanation for this is that the finite width of the two ρ suppresses the $\rho\rho$ signal slightly in the mass range available in $p\overline{p} \to$ annihilation to the $f_2(1565)$.

8 Interpretation

The $I = 0$ members of the $q\overline{q}$ 2^+ ground-state nonet are filled by $f_2(1270)$ and $f_2'(1525)$. The strong production rate of the $f_2(1565)$ makes it unlikely to be an $s\overline{s}$ state. It is not a good glueball candidate, since it has not been observed significantly in glue-rich channels. The most obvious possibility is that it is the radial excitation of $f_2(1270)$. In recent work on annihilation in flight, further f_2 resonances have been identified at 1945 ± 30 MeV and at 2210 ± 45 MeV [17]. The first of these resonances agrees with earlier observations of an f_2 by GAMS [9] and VES [9] groups at 1920 MeV. A straight line trajectory through these resonances as a function of s predicts a first radial excitation at 1630 MeV. This is close to the value found here. The $\omega\omega$ threshold may attract the resonance to a slightly lower mass. An $I = 1$ partner has been identified in Crystal Barrel data on $\bar{p}p \to \eta\eta\pi^0$ at 1940 MeV/c [18]. It has a mass of 1660 ± 40 MeV and a width of 280 ± 70 MeV.

An alternative identification of the AX is that it is a $q\overline{q}q\overline{q}$ state. However, such a state is not expected below 1800 MeV and is predicted to be very broad. A third possibility is that it is a molecule of $\omega\omega$; however, the binding of a 0^+ $\omega\omega$ molecule should be a factor 6 stronger [7], and there is no evidence for such a state.

8.1 Conclusion

It has been possible in this analysis, by using the two Crystal Barrel data sets of $\omega\omega\pi^o$ and $3\pi^o$, to determine important information about $f_2(1565)$. The $\omega\omega\pi^o$ data demand a dominant contribution from $f_2(1565)$; the branching fractions from $^1S_0$, $^3P_2$, $^3P_1$ are well determined. The contribution from P-state dominates strongly, partly because S-state production is suppressed by the centrifugal barrier for production.

The $3\pi^o$ data also demand a small contribution from $f_2(1565)$, both in S-state and P-state annihilation. Using the very well determined and stable branching fractions of the $f_2(1565)$ from the $\omega\omega\pi^o$ data, it has been possible to solve the problems found in previous analyses when introducing production of $f_2(1565)$ from P-state in the $3\pi^o$ data.

Using the Flatté form described earlier, the value of the mass determined by the fit is $1598 \pm 11(stat) \pm 9(syst)\, MeV$ and the value of the full width at half maximum of the summed cross section for $\pi\pi$, $\omega\omega$ and $\rho\rho$ channels is

220 ± 15 MeV. Systematic errors are due to uncertainty in the values of the radius of the centrifugal barrier and of the relationship between g_1 and g_2.

By unfolding the effects of the centrifugal barrier, it has been shown that the 2π width is very small, of the order of 2% of the average of the dominant $\rho\rho$ width. $\Gamma_{2\pi}$ was found to be 2.4 MeV with an uncertainty of a factor 3. This small value is due to the small branching fraction for $f_2(1565) \rightarrow \pi\pi$ seen in the $3\pi^o$ data. Table 14 shows the final values of the parameters used for $f_2(1565)$.

The use of incomplete parameterisations for the AX in previous work may account for the difference in masses and widths which have been found. In turn this explains the mis-identification of the AX as two distinct resonances, $f_2(1565)$ and $f_2(1640)$. The work in this thesis confirms that there is only one resonance with a mass around 1600 MeV.

Parameter	Value
Mass	1598(MeV)
g_1	1305 (MeV)
g_2	435 (MeV)
$\Gamma_{2\pi}$	2.4 (MeV)

Table 14: Final values of parameters used for $f_2(1565)$

9 Appendix 1: Formulae for resonance production

9.1 Quantisation axes

In the analysis of $p\overline{p} \rightarrow \omega\omega\pi^o$ two possible production mechanisms for resonant states are considered. The first is $p\overline{p} \rightarrow X\pi^o$ with $X \rightarrow \omega\omega$ (figure 1) and the second is $p\overline{p} \rightarrow X\omega$ with $X \rightarrow \omega\pi^o$ (figure 2).

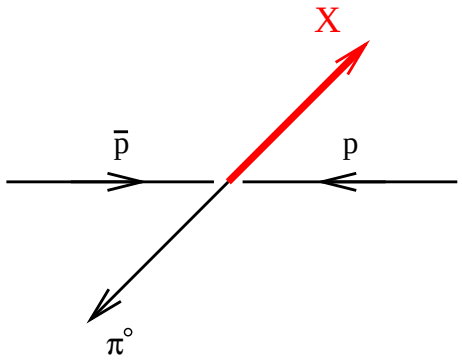

Figure 1: Production of resonance decaying to $\omega\omega$

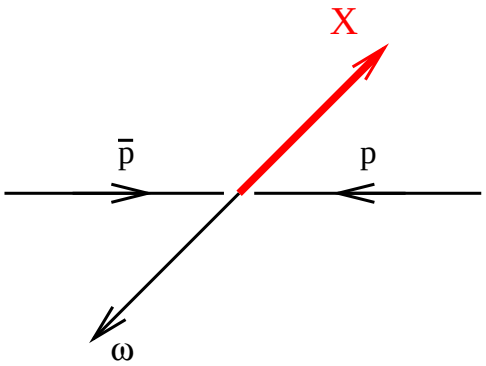

Figure 2: Production of resonance decaying to $\omega\pi^o$

The initial $p\overline{p} \rightarrow$ system is unpolarised, therefore any lab axes can be chosen for quantisation. For processes of the type $p\overline{p} \rightarrow X\pi^o$ it is convenient

to choose the $\pi^o X$ axes where the state vectors for X can be written easily. These state vectors are invariant under a Lorentz boost to the rest frame of X - so a boost is performed.

The spin information of the resonant state X is contained in the angular information and correlation of the decays of the ω's. The expressions for these decays are more easily evaluated in the $\omega\omega$ axes. So a rotation to these axes is performed and quantum mechanical rotation matrices are used to transform the state vectors from the $\pi^o X$ axes to the $\omega\omega$ axes.

In theory, for processes of the type $p\overline{p} \rightarrow X\omega$ the same axes should be used but because the only initial state we consider is $J = 0$ it is possible to rotate to any other axes with a rotation matrix of 1. Hence to simplify the expressions a rotation to the ωX axes is applied plus a boost to the rest frame of X. The fact that the initial spin is zero also allows the axes for the two cases (i.e. decay to either ω) to be separated. For this process instead of using rotation matrices to rotate to the $\omega\pi^o$ axis a Wick rotation was used.

9.2 The matrix element for $\omega \rightarrow \pi^+\pi^-\pi^o$

The decay of the ω meson to $\pi^+\pi^-\pi^o$ can be considered to be a two body process, $\omega \rightarrow R\pi$ where R is a resonance decaying to a pion pair and the other pion is a spectator. There are three possibilities for which two pions make up R, $R \rightarrow \pi^+\pi^-$, $\pi^+\pi^o$ or $\pi^-\pi^o$. However $R \rightarrow \pi^+\pi^-$ is forbidden by C-parity conservation and can be discounted.

The ω meson has $J^P = 1^-$ and the pions each have $J^P = 0^+$, J,P and isospin conservation require the ω to decay to R with $J = 1$ and a spectator pion which has $\ell = 1$.

$\ell = 1$ decays are described (in the overall centre of mass) by momentum vectors $\mathbf{p}$ e.g.$|S_R = 1, S_{Rz} = 1 >$ is described by $pcos\theta = p_z$; the $cos\theta$ factor appears from the angular dependence of the orbital angular momentum and the factor p comes from the factor $\mathbf{p}^s$ for the phase space of the decay.

Hence $R \rightarrow \pi^-\pi^o$ is described by $\mathbf{p}^+$- $\mathbf{p}^0$ (where $\mathbf{p}^+$,$\mathbf{p}^-$ and $\mathbf{p}^0$are the momenta vectors of the π^+, π^- and π^o respectively). $R \rightarrow \pi^o\pi^-$ is also described by $\mathbf{p}^+$-$\mathbf{p}^0$ due to the change of sign of the wave function under interchange of the particles. $R \rightarrow \pi^-\pi^o$ is described by $\mathbf{p}^-$- $\mathbf{p}^0$. The spectator pion is described by its momentum vector.

As the ω is a vector particle the vectors describing R and the spectator must be combined in such a way as to give a resultant vector. The simplest way to do this is to take their cross product.

For the case $R \rightarrow \pi^+\pi^o$ with π^- as the spectator the ω is described by $(\mathbf{p}^+ - \mathbf{p}^0) \times \mathbf{p}^-$. Using the fact that due to momentum conservation $\mathbf{p}^+ + \mathbf{p}^- + \mathbf{p}^0 = 0$ it is possible to substitute for $\mathbf{p}^-$, giving:

$$(\mathbf{p}^+ - \mathbf{p}^0) \times -(\mathbf{p}^+ + \mathbf{p}^0) = 2(\mathbf{p}^0 \times \mathbf{p}^+) \tag{25}$$

Equivalently for the case $R \rightarrow \pi^-\pi^o$ the result is $-2(\mathbf{p}^0 \times \mathbf{p}^-)$.

Hence the matrix element for the ω decay may be described by:

$$\frac{2.2}{\sqrt{6}}[(\mathbf{p}^0 \times \mathbf{p}^+) - (\mathbf{p}^0 \times \mathbf{p}^-)] \tag{26}$$

where the factor $\sqrt{6}$ comes from Clebsch-Gordan coefficients for the decays of the ω and R. Once again using momentum conservation this simplifies to:

$$\frac{8}{\sqrt{6}}[\mathbf{p}^+ \times \mathbf{p}^-] \tag{27}$$

In fact it is possible to form the matrix element using the cross product of any of the three pions (using momentum conservation); however $\mathbf{p}^+$ and $\mathbf{p}^-$ were chosen because angular information on charged particles in the Crystal Barrel detector is better determined than for neutral particles).

Absorbing the factor $\frac{8}{\sqrt{6}}$ into the overall normalisation constant the matrix element for $\omega \rightarrow \pi^+\pi^-\pi^o$ becomes:

$$\begin{pmatrix} \omega_x \\ \omega_y \\ \omega_z \end{pmatrix} = \begin{pmatrix} p_y^+ p_z^- - p_z^+ p_y^- \\ p_z^+ p_x^- - p_z^- p_x^+ \\ p_x^+ p_y^- - p_y^- p_x^+ \end{pmatrix} = \begin{pmatrix} n_x \\ n_y \\ n_z \end{pmatrix} \tag{28}$$

where $\mathbf{n} = \mathbf{p}^+ \times \mathbf{p}^-$.

As it is a vector particle, the ω behaves (under $SU2$) like the Legendre polynomial with $L = 1$. The latter is described by:

$$P_1^1(\theta, \phi) \quad \alpha \quad -sin\,\theta e^{i\phi} \tag{29}$$

$$P_0^1(\theta, \phi) \quad \alpha \quad \sqrt{2}\,cos\,\theta \tag{30}$$

$$P_{-1}^1(\theta, \phi) \quad \alpha \quad sin\,\theta e^{-i\phi} \tag{31}$$

therefore the matrix elements for an omega with $m = 1$ (ω_1), $m = 0$ (ω_0) and $m = -1$ (ω_{-1}) are:

$$\omega_1 = -(\omega_x + i\omega_y) \quad (32)$$
$$\omega_0 = \sqrt{2}\omega_z \quad (33)$$
$$\omega_{-1} = (\omega_x - i\omega_y). \quad (34)$$

Using this result, it is possible to derive expressions for the matrix elements for production of the different resonances possible in terms of $\mathbf{n}$. These expressions have been derived before for the case when the ω decays to $\pi^o\gamma$ giving an 8γ final state and are detailed in CB-note 293 [19]. The only difference between the case $\omega \to \pi^o\gamma$ and the case $\omega \to \pi^+\pi^-\pi^o$ is that for the former there is a summation over the four polarisation states of the 2γ's from the ω decays. Therefore the reader is advised to look there for further details.

References

[1] C. Amsler et al., Phys. Lett. 327B (1994) 425.

[2] B. May et al., Phys. Lett. B225 (1989) 450.

[3] B. May et al., Z. Phys. C46 (1990) 203.

[4] V.V. Anisovich et al., Phys. Lett. B323 (1994) 233.

[5] C. Amsler et al., Phys. Lett. B355 (1995) 425.

[6] A. Adamo et al., Nucl. Phys. A558 (1993) 13C.

[7] A. Abele et al., Nucl. Phys. A609(1996) 562.

[8] D. Alde et al., Phys. Lett. B241 (1990) 600.

[9] A. Beladidze et al., Z. Phys. C54 (1992) 367.

[10] Particle Data Group, Euro. Phys. J. 3 (1998) 1.

[11] Zemach, Phys. Rev. B140 (1965) 97.

[12] D.V. Bugg et al., Phys. Lett. B353 (1995) 378.

[13] U. Thoma, AIP Conf. Proc. 432 (1998) 322.

[14] D.V. Bugg, A.V. Sarantsev and B.S. Zou, Nucl. Phys. B471 (1996)

[15] B. Hyams et al., Nucl. Phys. B64 (1973) 134.

[16] J. Vandermeulen, Z. Phys. C37 (1988) 563.

[17] A.Anisovich et al., submitted to Nucl. Phys. A.

[18] A. Abele et al., submitted to Zeit. Phys. C.

[19] C.Pinder, D.V.Bugg and C.Hodd, CB-note 293 (1996)

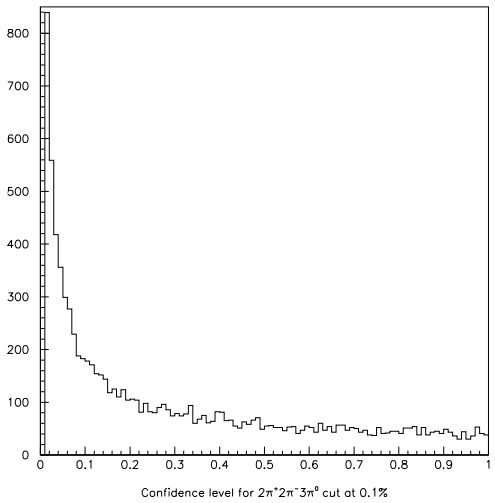

Figure 3: Confidence level distribution for $2\pi^+2\pi^-3\pi^o$ hypothesis cut at 0.1% (data)

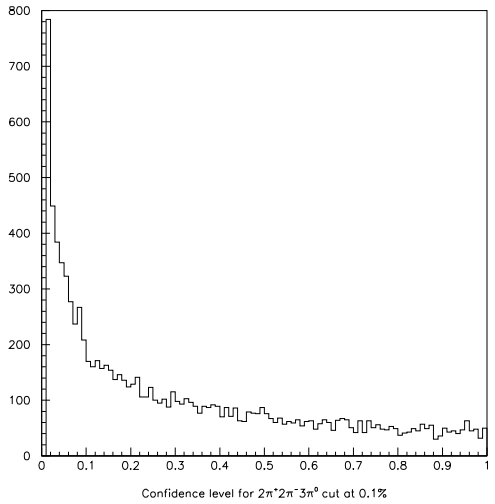

Figure 4: Confidence level distribution for $2\pi^+2\pi^-3\pi^o$ hypothesis cut at 0.1% (Monte Carlo)

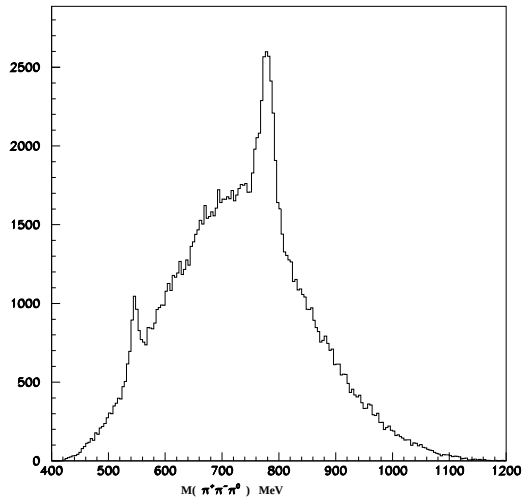

Figure 5: Invariant mass of $\pi^+\pi^-\pi^o$ combinations for $2\pi^+2\pi^-3\pi^o$ hypothesis

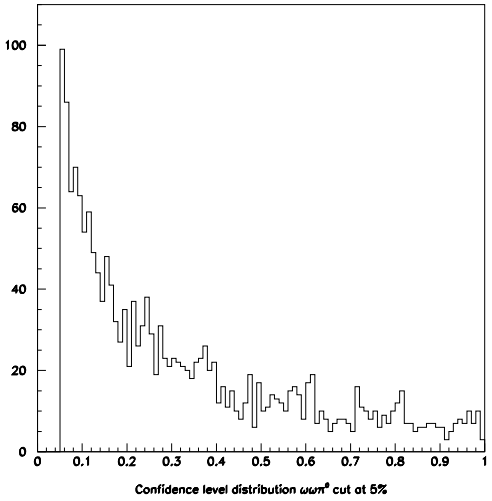

Figure 6: Confidence level distribution for $\omega\omega\pi^o$ hypothesis cut at 5% (data)

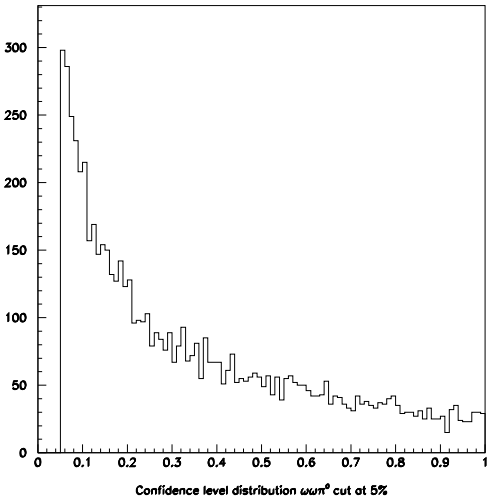

Figure 7: Confidence level distribution for $\omega\omega\pi^o$ hypothesis cut at 5% (Monte Carlo)

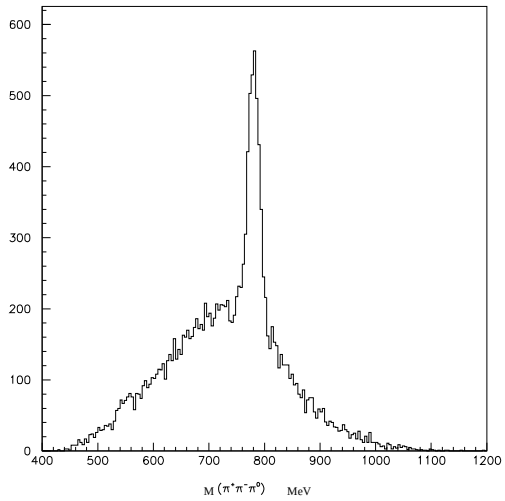

Figure 8: Invariant mass of $\pi^+\pi^-\pi^o$ combinations for $\omega\omega\pi^o$ hypothesis

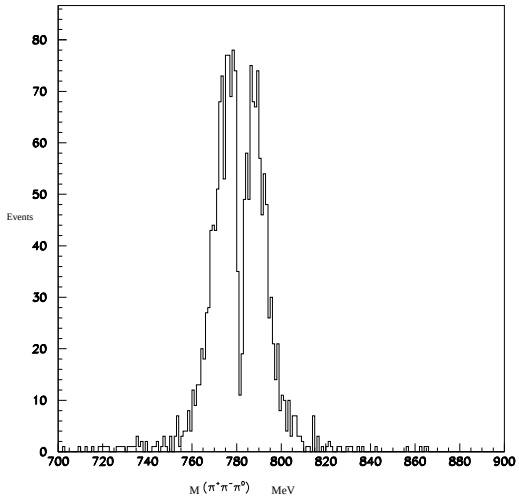

Figure 9: M($\pi^+\pi^-\pi^o$) distribution of the second best omega (data)

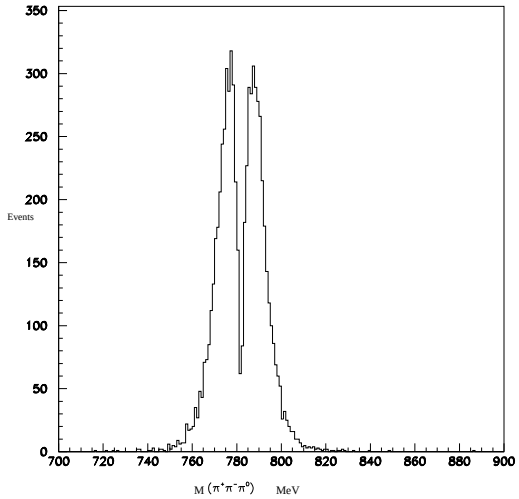

Figure 10: M($\pi^+\pi^-\pi^o$) distribution of the second best omega (Monte Carlo)

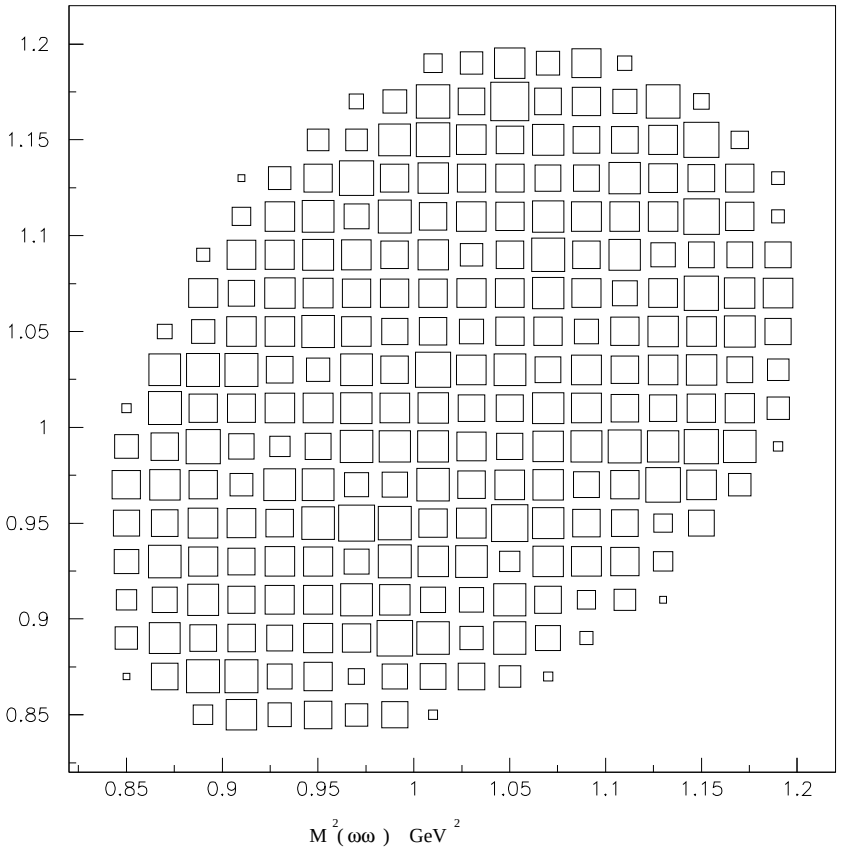

Figure 11: Dalitz plot for Monte Carlo events

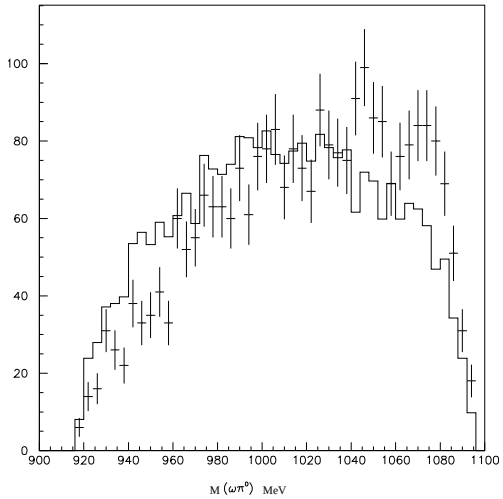

Figure 12: Comparison with phase space for $\omega\pi^o$, error bars are data, the histogram is phase space

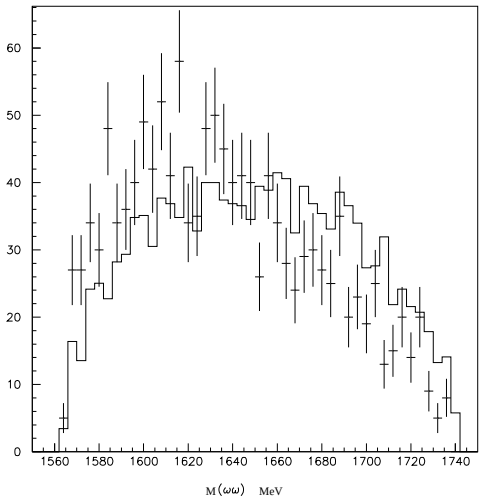

Figure 13: Comparison with phase space for $\omega\omega$, error bars are data, the histogram is phase space

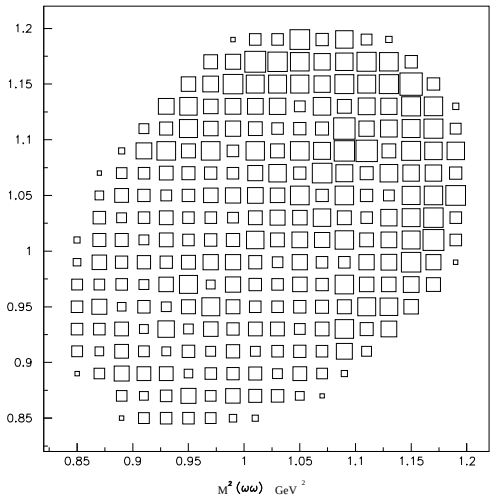

Figure 14: Dalitz plot for data

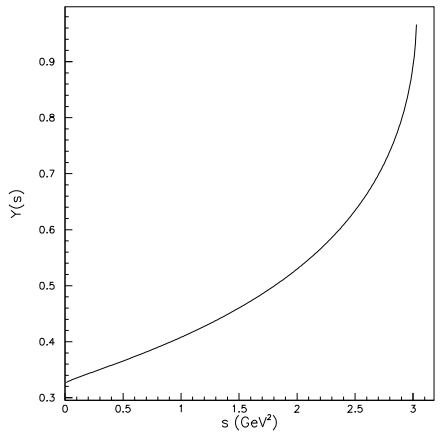

Figure 15: The Vandermeulen form factor as a function of s.

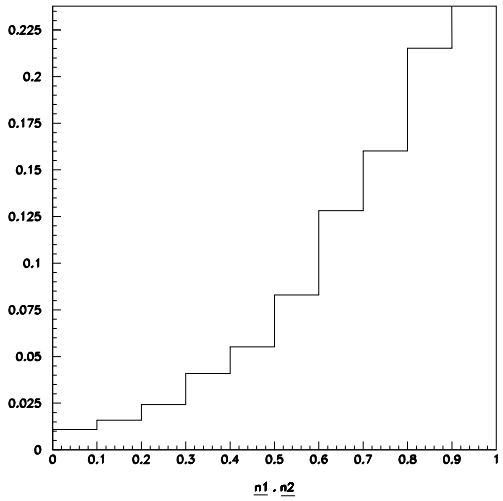

Figure 16: $\underline{n_1}.\underline{n_2}$ distribution for a 0^+ resonance

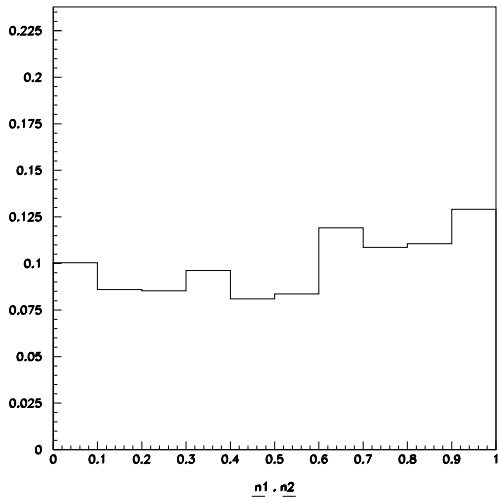

Figure 17: $\underline{n_1}.\underline{n_2}$ distribution for a 2^+ resonance

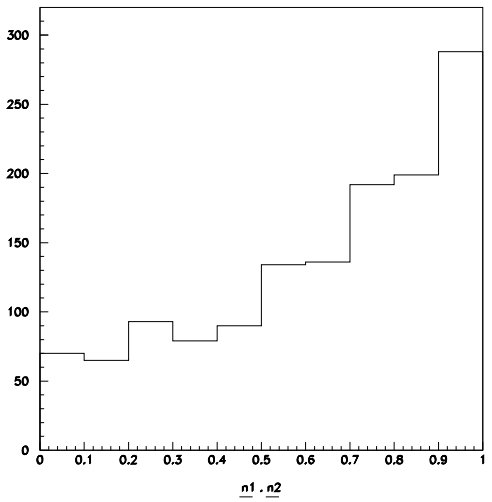

Figure 18: $\underline{n_1}.\underline{n_2}$ distribution of the data

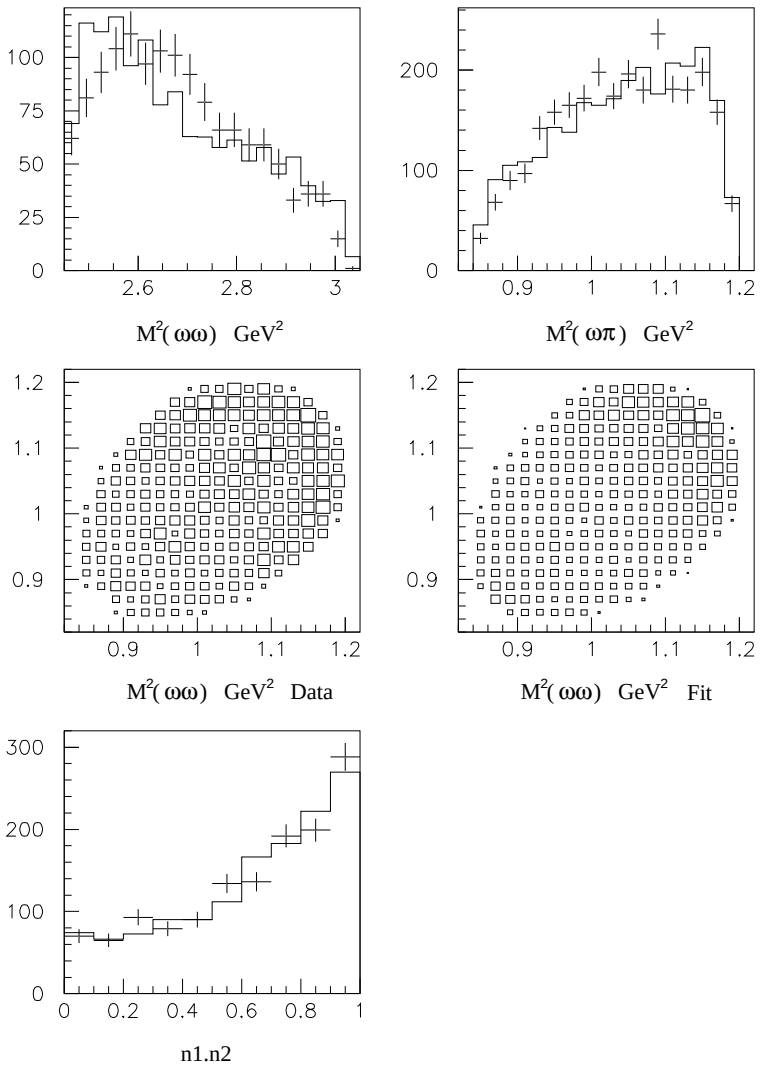

Figure 19: Projections for reference fit

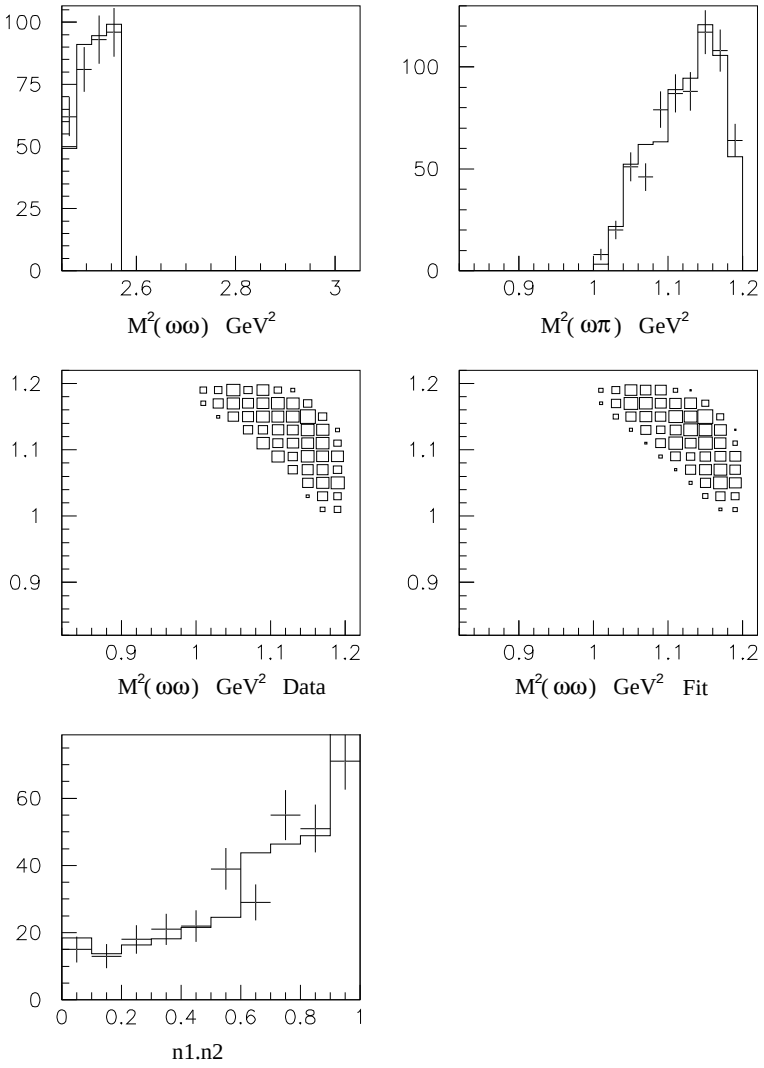

Figure 20: Projections for first mass slice

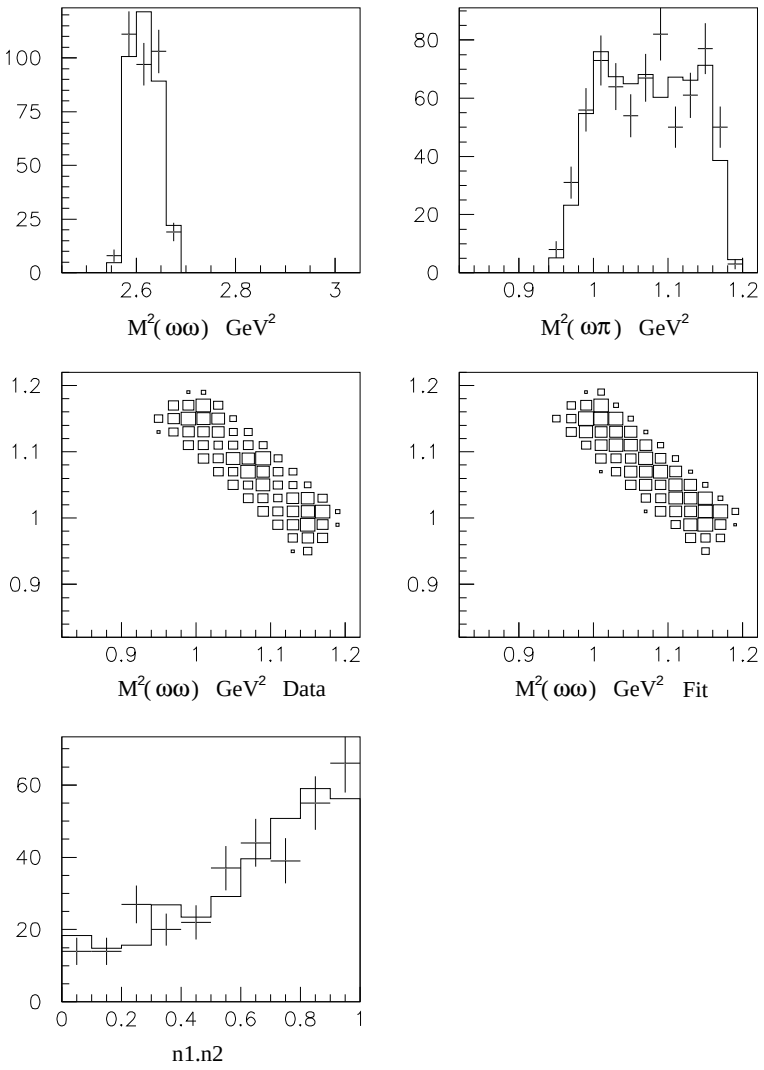

Figure 21: Projections for second mass slice

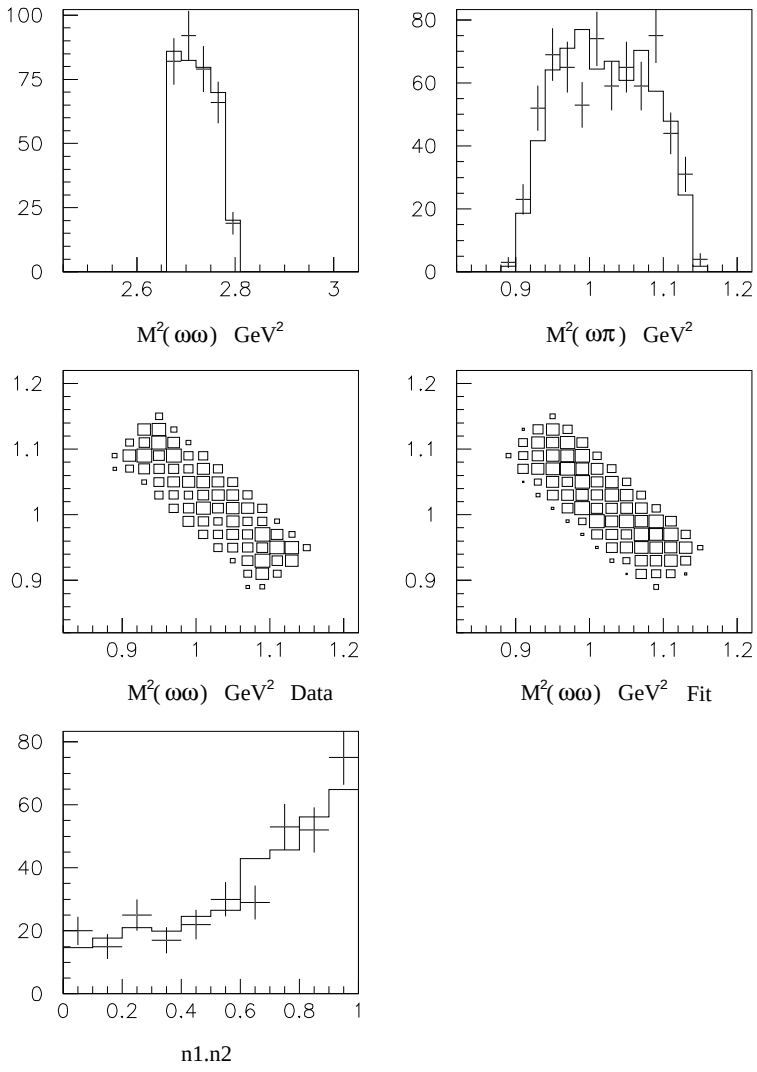

Figure 22: Projections for third mass slice

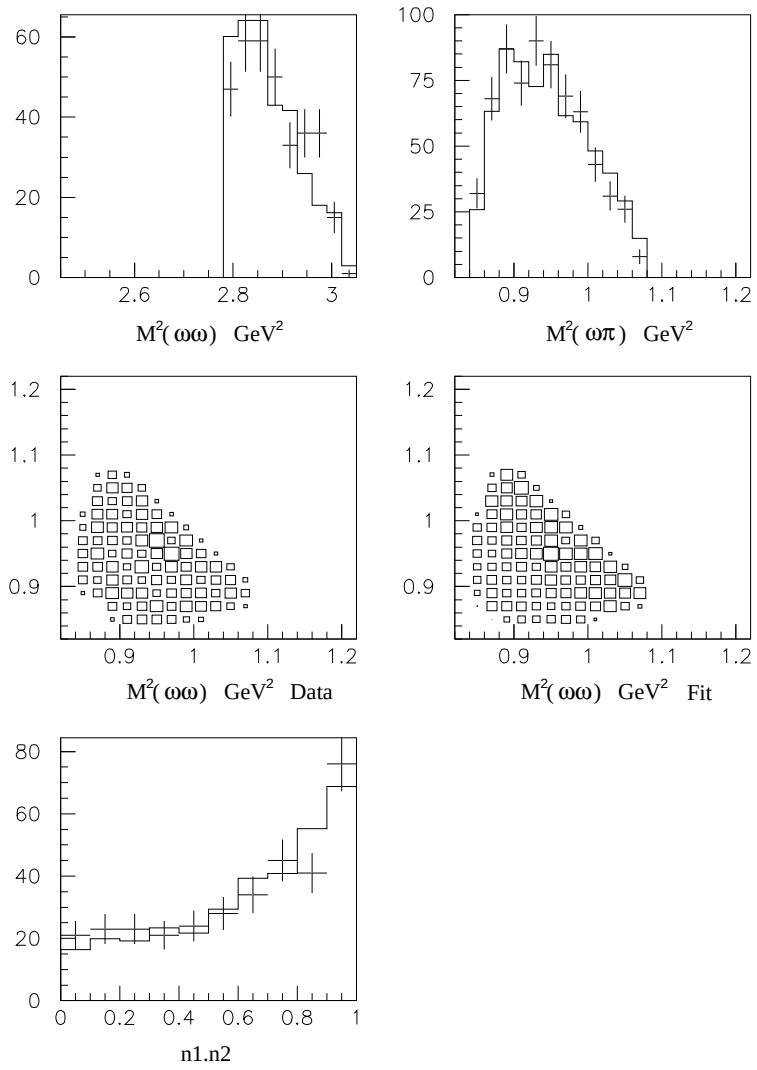

Figure 23: Projections for fourth mass slice

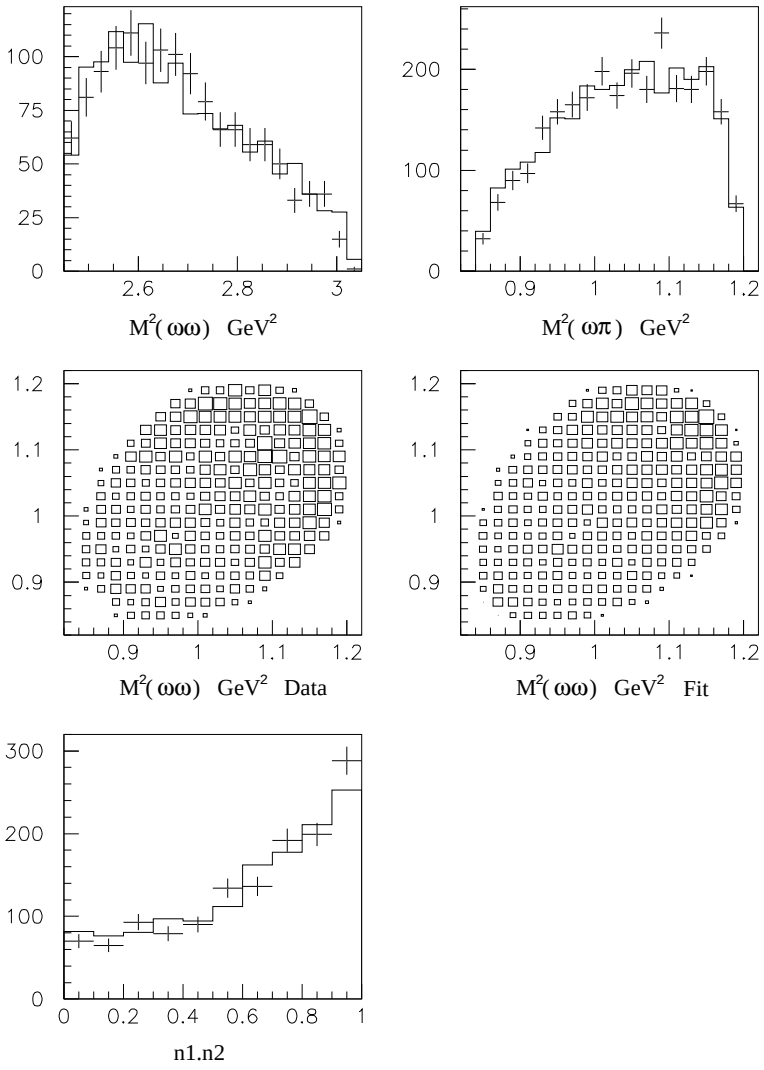

Figure 24: Projections for fit with $\Gamma = 202\ MeV$, $M = 1565\ MeV$ for $f_2(1565)$

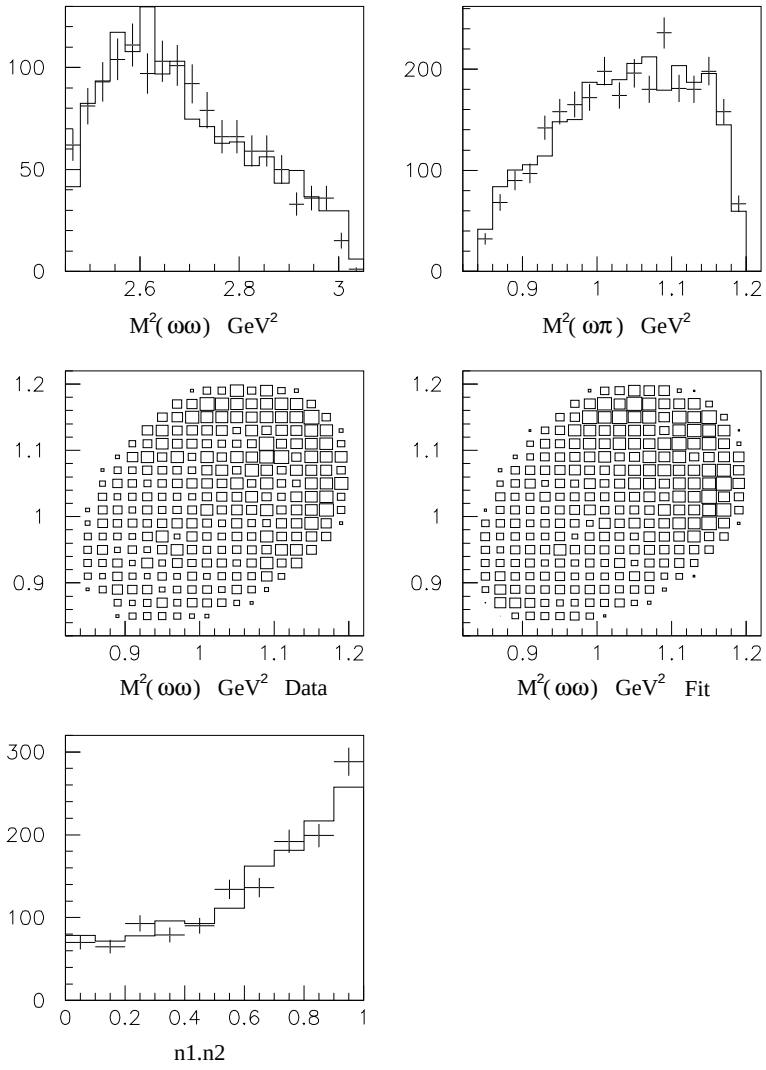

Figure 25: Projections for fit with $\Gamma = 102\ MeV$, $M = 1605\ MeV$ for $f_2(1565)$

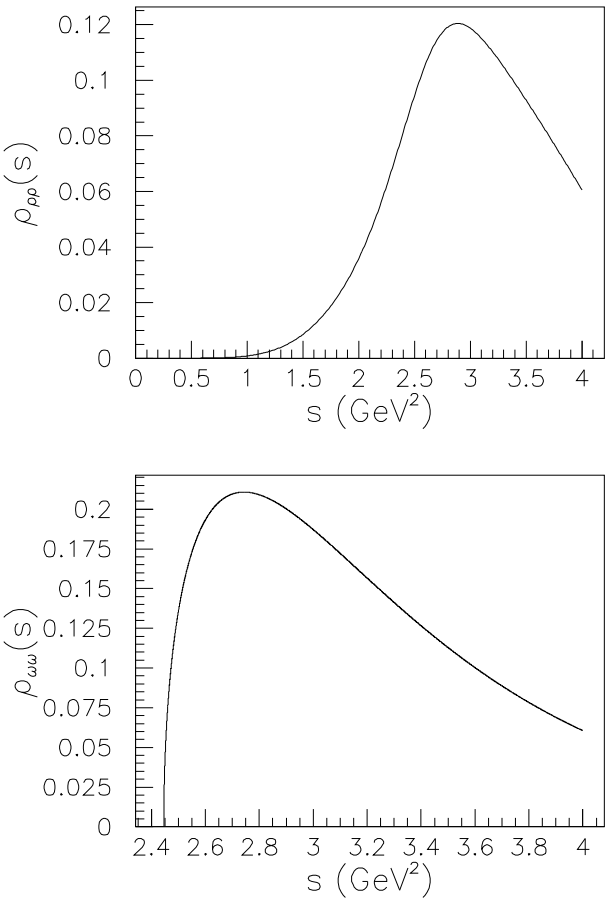

Figure 26: (a) The phase space factor for $\rho\rho$ as a function of s; (b) for $\omega\omega$.

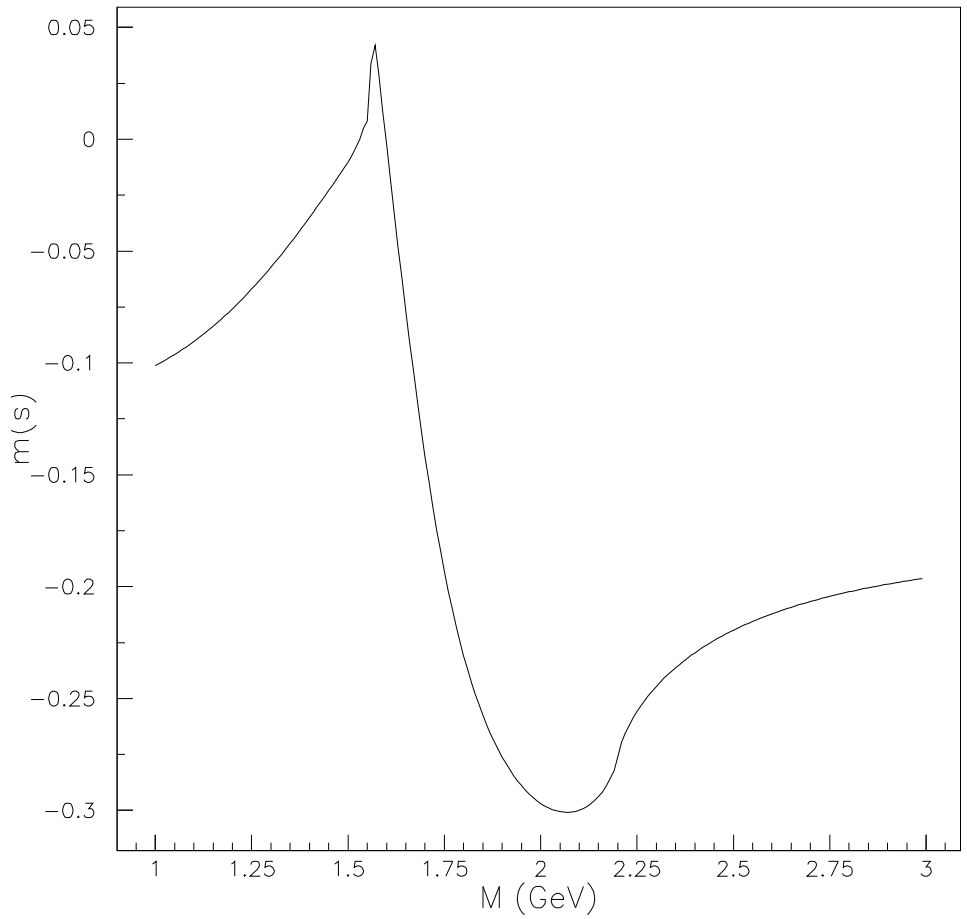

Figure 27: The dispersive correction to the mass ($m(s)$) as a function of s

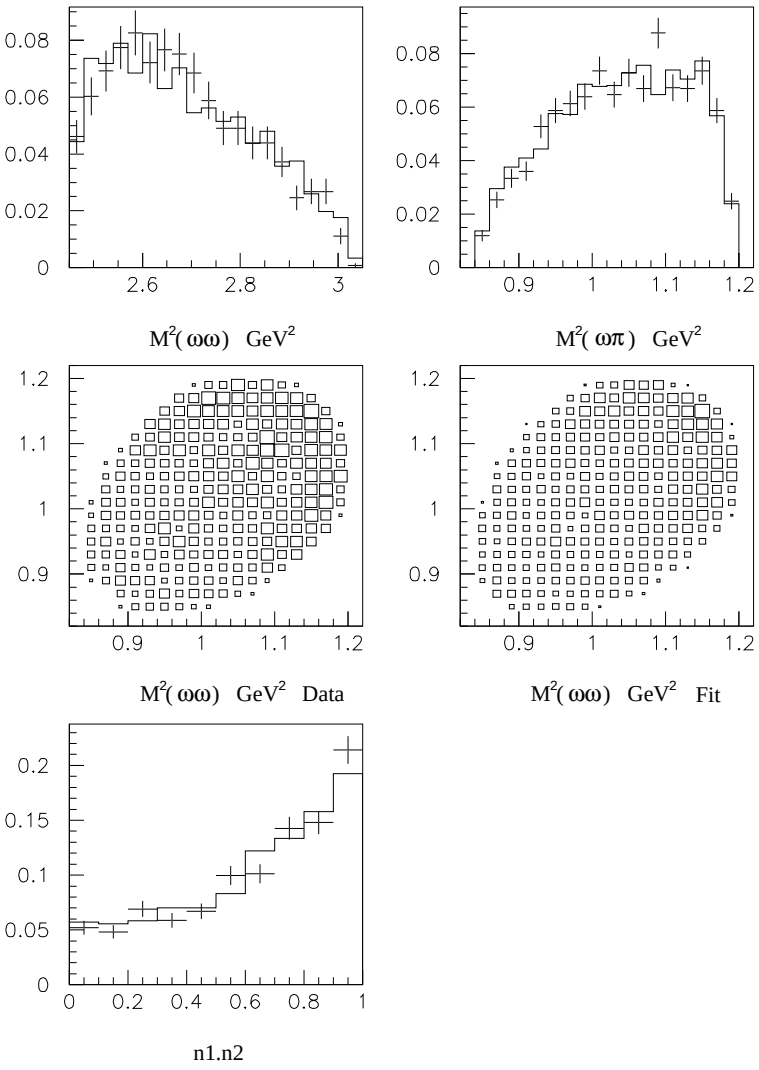

Figure 28: Projections for Flatté $f_2(1565)$ with mass of 1605 MeV, $g_2 = 430$ MeV, $\Gamma_{\pi\pi} = 30$ MeV

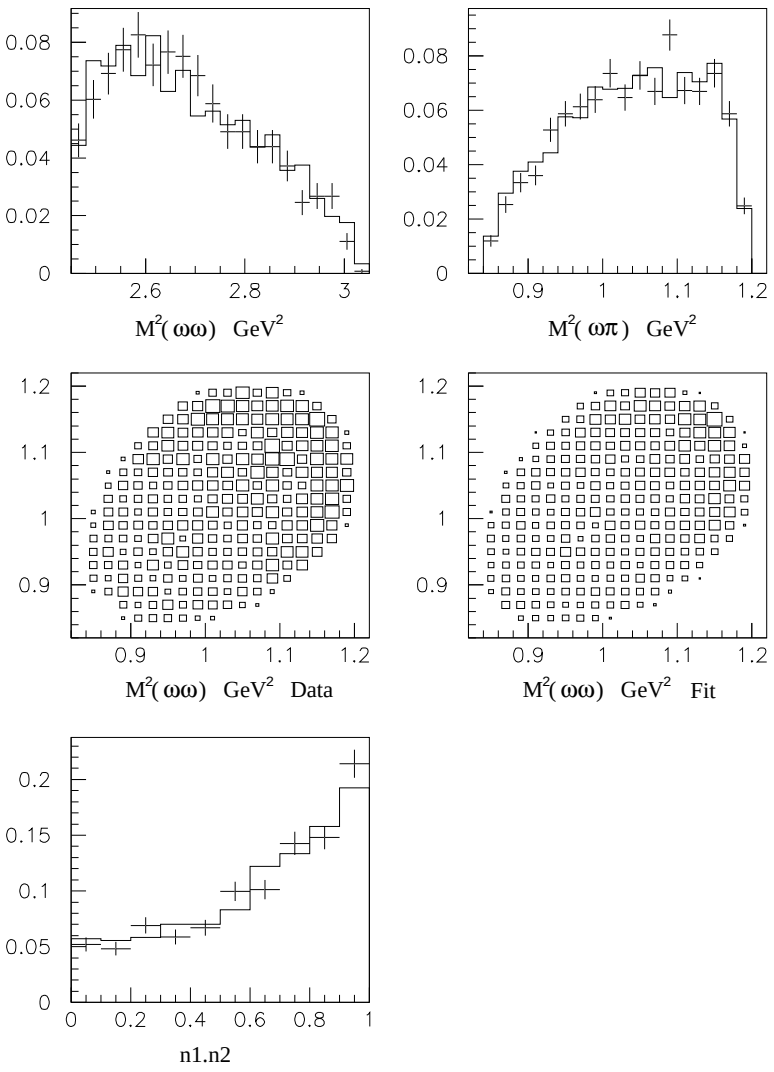

Figure 29: Projections for combined fit with $3\pi^o$ data using the Flatté form; $f_2(1565)$ has mass of 1598 MeV, $g_2 = 435\ MeV$, $\Gamma_{\pi\pi} = 2.4\ MeV$

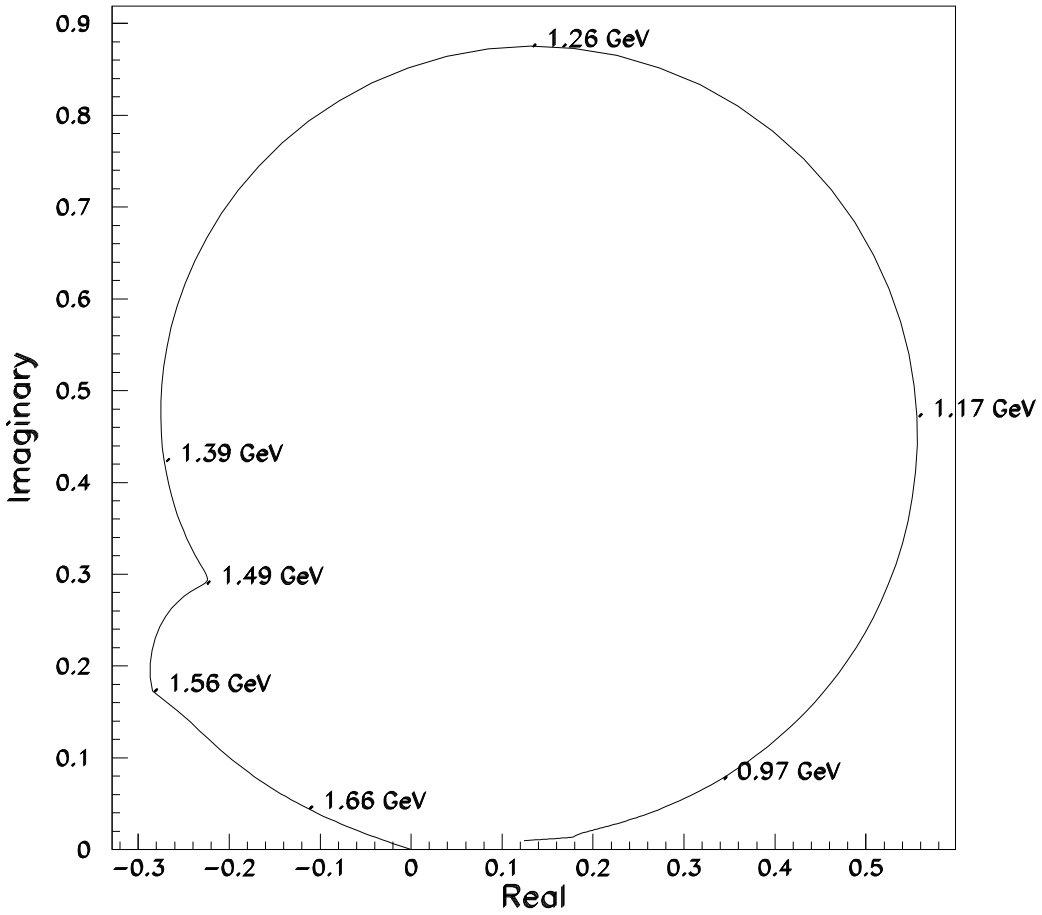

Figure 30: Argand diagram for the $\pi\pi$ D-wave fitted to $3\pi^0$ data

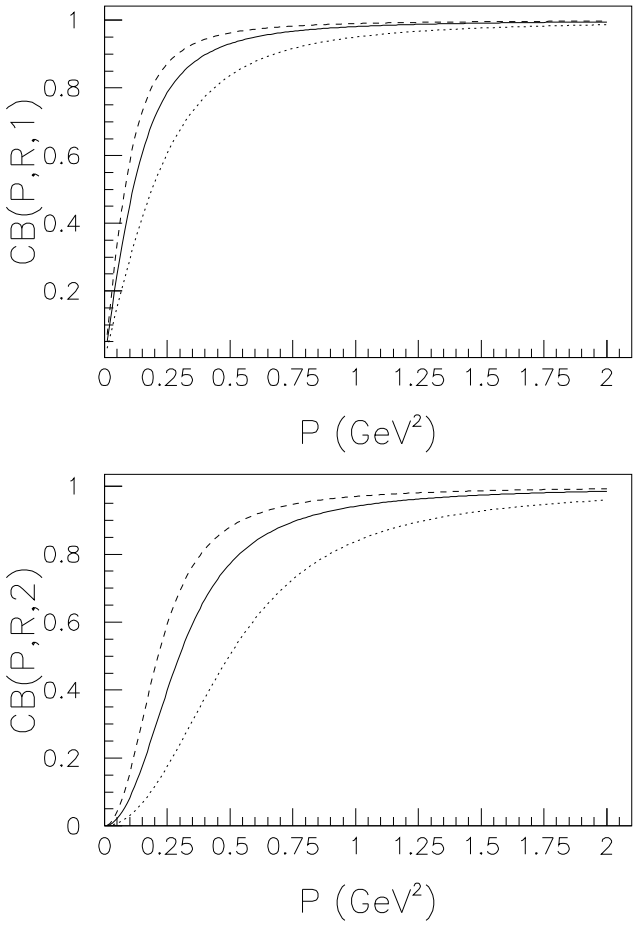

Figure 31: (a) Centrifugal barrier factor for l=1 as a function of P , for R=1.0 (full), 1.4 (dashed), 0.6 (dotted); (b) as (a) but for l=2

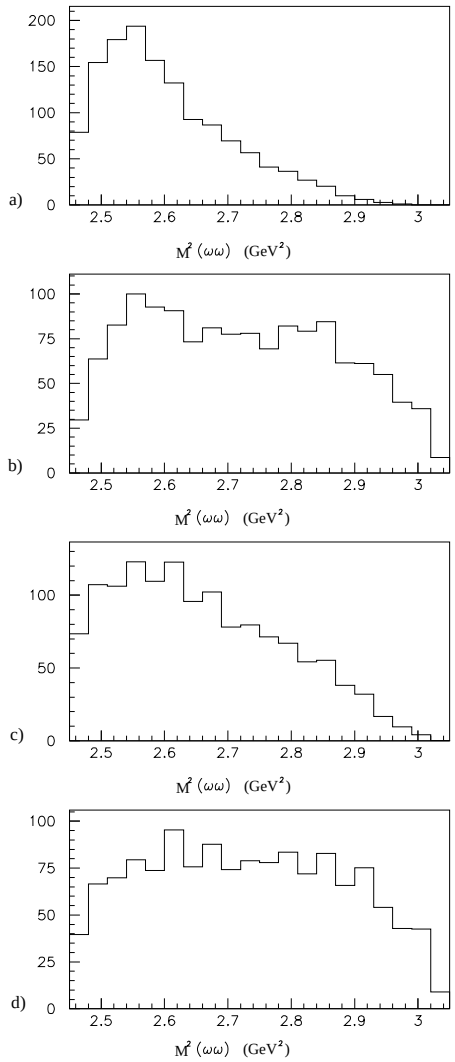

Figure 32: The contribution to the $\omega\omega$ projection from $f_2(1565)$ (a) from $^1S_0$; (b) from $^1S_0$ omitting the centrifugal barriers; (c) from P-state; (d) from P-state omitting the centrifugal barriers.

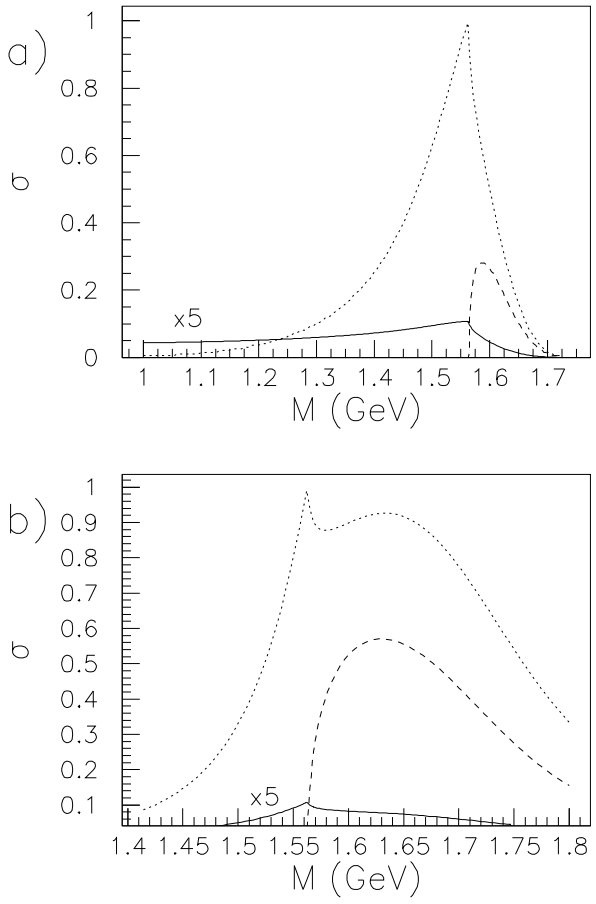

Figure 33: (a) The intensity distribution for $f_2(1565) \to \pi\pi$ (full curve), $\omega\omega$ (dashed) and $\rho\rho$ (dotted) for production in $\bar{p}p$ annihilation from $^1S_0$; the $\pi\pi$ ratio has been scaled up by a factor 5 to make it clearly visible; (b) as (a) for the $f_2(1565)$ uninhibited by the phase space for production in $\bar{p}p$ annihilation or centrifugal barrier factors. Units of the vertical axis are arbitrary.